THESIS FOR THE DEGREE OF DOCTOR OF PHILOSOPHY

Development of Novel *In Situ* Microscopy Techniques for the Study of Water Interaction with Soft Materials

ANNA JANSSON

Department of Applied Physics

CHALMERS UNIVERSITY OF TECHNOLOGY

Gothenburg, Sweden 2014

Development of Novel *In Situ* Microscopy Techniques for the Study of Water Interaction with Soft Materials
ANNA JANSSON
ISBN 978-91-7597-120-9

Doktorsavhandlingar vid Chalmers tekniska högskola
Ny serie nr 3801
ISSN 0346-718X

Department of Applied Physics
Chalmers University of Technology
SE-412 96 Gothenburg
Sweden
Telephone: +46 (0)31 772 10 00
Fax: +46 (0)31 772 32 24

The figure on the cover shows ESEM images of the internal microstructure of a porous polymer film for controlled-release applications (top), a yeast cell in contact with an AFM probe (middle) and a cellulose fibre in contact with a water droplet (bottom).

Printed by:
Chalmers Reproservice
Gothenburg, Sweden 2014

Development of Novel *In Situ* Microscopy Techniques for the Study of Water Interaction with Soft Materials

ANNA JANSSON
Department of Applied Physics
Chalmers University of Technology

ABSTRACT

The transport of water in soft materials can occur in liquid or gas phase and is highly dependent on the material microstructure and the structure dynamics. Understanding these relationships is the basis for the development of predictive models that can aid the design of new and improved functional materials. The environmental scanning electron microscope (ESEM) enables the visualisation of the effects of hydration or dehydration on a specimen down to the nanometre scale, facilitating the understanding of the structure-property relationships. However, the full potential of the ESEM has not yet been explored, especially when it comes to the transport of water in materials.

The aim of this work was to develop new ESEM-based methods that enable the *in situ* study of water interaction with soft materials in a controlled manner. We designed a sample stage that uses a manipulator to bring the specimen in contact with a water reservoir in the ESEM, rendering the point of contact between water and specimen available for visual studies. In addition, coupled with a piezoresistive atomic force microscopy (AFM) sensor, the setup enables the local measurement of displacements in the nanometre range with millisecond temporal resolution through force spectroscopy. Thus, it provides a sensitive probe for swelling, which is an important effect of the water interaction for many soft materials. The potential of the developed methods has been demonstrated on three different materials systems and geometries.

The absorption and transport of liquid water in individual cellulose fibres were imaged for the first time. The volumes of absorbed droplets were typically in the range of 0.02 nL to 0.2 nL and the rate of absorption varied between different fibres. The method was also applied to phase-separated polymer films intended as controlled-release coatings in oral pharmaceutical formulations and enabled the first studies of the water interaction in the initial stage of wetting. Simultaneous probing of the microstructure and the local water transport properties of the films provided previously inaccessible information about the structure-transport relationships and the microstructural evolution caused by the water interaction. In addition, measurements of the time-dependent osmotic swelling of yeast cells in the ESEM were demonstrated with a high spatial and temporal resolution. This type of measurement is valuable for the understanding of the water transport properties of cell membranes. The versatility of the setup allows the technique to be applied to a wide range of different materials systems and geometries where the interaction with water is of interest.

Keywords: environmental scanning electron microscopy, in situ, manipulator, water interaction, water transport, swelling, cellulose fibre, polymer film, yeast cell, osmotic shock

PREFACE

The research presented in this thesis was carried out in the Division of Microscopy and Microanalysis and in the Eva Olsson group in the Department of Applied Physics, Chalmers University of Technology, Gothenburg, Sweden, during the periods of March 2009 through February 2011 and January 2012 through December 2014, under the supervision of Prof. Eva Olsson and assistant supervisors Dr. Stefan Gustafsson and Prof. Anne-Marie Hermansson.

The following papers are included in this thesis:

Paper I. **Novel Method for Controlled Wetting of Materials in the Environmental Scanning Electron Microscope**
A. Jansson, A. Nafari, A. Sanz-Velasco, K. Svensson, S. Gustafsson, A.-M. Hermansson, and E. Olsson

Microscopy and Microanalysis 2013, 19(1), 30-37

Paper II. **Monitoring the Osmotic Response of Single Yeast Cells Through Force Measurement in the Environmental Scanning Electron Microscope**
A. Jansson, A. Nafari, K. Hedfalk, E. Olsson, K. Svensson and A. Sanz-Velasco

Measurement Science and Technology 2014, 25, 025901 (8pp)

Paper III. **Novel Method for Visualising Water Transport Through Phase-Separated Polymer Films**
A. Jansson, C. Boissier, M. Marucci, M. Nicholas, S. Gustafsson, A.-M. Hermansson and E. Olsson

Microscopy and Microanalysis 2014, 20(2), 394-406

Paper IV. **Dynamics of Water Transport Through Polymer Films Studied by a Novel *In Situ* ESEM Approach**
A. Jansson, C. Boissier, M. Marucci, M. Nicholas, S. Gustafsson, A.-M. Hermansson and E. Olsson

Manuscript intended for Soft Matter

My contribution to the appended papers:

Paper I: I co-developed the experimental setup, did all the experimental work, carried out the evaluation in discussion with my co-authors and wrote the paper.

Paper II: I co-developed the experimental setup, did the microscopy work and evaluation together with my co-authors, and was the main author of the paper.

Paper III: I did all the experimental work, carried out the evaluation in discussion with my co-authors and wrote the paper.

Paper IV: I did all the ESEM-related work, participated in the TEM work together with my co-authors, carried out the evaluation in discussion with my co-authors and wrote the paper.

In addition to the above papers, I have contributed to the following work, which is not included in this thesis:

Characterisation of pore structure of polymer blended films used for controlled drug release

H. Häbel, H. Andersson, A. Jansson, E. Olsson, A. Larsson and A. Särkkä
Manuscript, 2014.

Anna Jansson
Gothenburg, December 2014

ABBREVIATIONS

AFM	Atomic force microscopy
DS	Degree of substitution
EC	Ethyl cellulose
ESEM	Environmental scanning electron microscope
FSP	Fibre saturation point
GSED	Gaseous secondary electron detector
HPC	Hydroxypropyl cellulose
HPMC	Hydroxypropylmethyl cellulose
HAADF	High angle annular dark field
MS	Molar substitution
PLA	Pressure-limiting aperture
RH	Relative humidity
RVP	Relative vapour pressure
SE	Secondary electron
SEM	Scanning electron microscope
STEM	Scanning transmission electron microscopy
SVP	Saturated vapour pressure
TEM	Transmission electron microscope

TABLE OF CONTENTS

1 INTRODUCTION

1.1 Background

The performance of many soft functional materials depends crucially on the interaction with water. For example, in hygiene products we rely on the ability to quickly absorb and transport liquids and the release of drugs from oral pharmaceuticals depends on the interaction of the product formulation with the aqueous environment in the body. On a basic level, the water transport properties of biological cell membranes are essential for cellular activities. The interaction of soft materials with water thus constitutes an important field of research. Here, "soft materials" refers to materials in the soft condensed matter category, a class of materials with a broad definition and properties intermediate between the solid and liquid state with respect to molecular organisation, intermolecular interactions and mechanical properties. Soft materials include, for example, complex liquids, polymers and biological materials (Riste & Sherrington, 1989; Löwen *et al*., 2000).

A few decades ago, the advent of the environmental scanning electron microscope (ESEM) opened up unique possibilities for studies of the interaction between materials and water at the micro- and nanometre scale. In contrast to the high vacuum requirement of a conventional scanning electron microscope (SEM), the ESEM is designed to operate in a gaseous environment at pressures of up to 20 torr. The presence of a gas enables imaging of electrically insulating specimens without the need to apply an electrically conducting coating. If the gas is water vapour, additional possibilities arise. By regulating the sample temperature and the water vapour pressure inside the sample chamber, the relative humidity (RH) at the sample site can be controlled. This means that water-containing materials can be stabilised and imaged in their native state, omitting the need for water removal procedures that may cause artefacts in the form of structural changes. The water vapour can also be used to perform dynamic *in situ* experiments involving the hydration or dehydration of specimens. (Donald *et al.*, 2000)

The ESEM has been extensively used to study different materials and a comprehensive review of the principles as well as some important applications is provided by Stokes (2008). The absence of conductive coatings on electrically insulating materials makes it possible to mechanically manipulate specimens without the constraints imposed by a coating (Thiel & Donald, 1992; Rizzieri *et al*., 2003). The response to hydration or dehydration can involve effects such as swelling, shrinking, dissolution or rearrangement of structures (Donald *et al.*, 2000; Jenkins & Donald, 2000; Montes-H *et al.*, 2005; Dragnevski & Donald, 2008). However, when it comes to the study of the transport of water through materials, reported ESEM applications are scarce. This may, in part, be attributed to limitations of the standard approach to wetting in the ESEM.

In situ wetting of a specimen in the ESEM is usually accomplished by increasing the RH to induce condensation onto the specimen surface. This can be done by increasing the water vapour pressure (alternatively decreasing the sample temperature) above the dew point (100% RH). For many applications involving liquid water transport, this

method does not offer sufficient control over the wetting process. Water condenses in the form of droplets or a continuous layer on the specimen surface, depending on the nature of the material. This means that the precise location of the point of interaction between water and specimen cannot be determined and controlled. Also the water is relatively opaque to the electrons used for imaging and therefore often obscures the underlying structure (Jenkins & Donald, 2000). These aspects render the traditional wetting approach generally inappropriate for studies of water transport and related effects on the microstructure.

There are examples of *in situ* techniques that address some of the limitations. For example, a better control of the point of interaction can be achieved by using a microinjector to locally dispense liquids onto the specimen surface (Danilatos & Brancik, 1968; Wei *et al.*, 2002; Wei *et al.*, 2003*a*; Camacho-Bragado *et al.*, 2011). However, work in this area is limited. Reingruber and co-workers (2012) used an innovative approach to study the wetting and drying of membranes in the ESEM, allowing the study of the transport of water in the liquid and gas phases inside the porous membrane structure. Alink and associates (2011) used two different methods to achieve *in situ* water transport through gas diffusion layers for fuel cells applications, where one involved a water reservoir under pressure and the other involved a temperature gradient applied across the sample. To the author's knowledge, no other methods for studying water transport in the ESEM have been presented.

In addition to water transport, swelling is an important aspect of water interaction. Many soft materials undergo swelling in aqueous or humid environments and the ESEM can be used to probe the local swelling of materials structures by imaging. However, measurements of the extent and rate of swelling in the ESEM can be limited by imaging-related aspects, especially for small structures that challenge the resolution of the microscope under given imaging conditions or during rapid events where the frame rate is limited by the maximum scanning speed that can be used without compromising image quality. Therefore, *in situ* techniques that enable measurements of local swelling at a high spatial and temporal resolution may aid the characterisation of certain materials and phenomena.

This work concerns the development of new *in situ* ESEM methods that enable the study of water interaction with soft materials in a controlled manner. We have developed a flexible experimental platform widely applicable to different materials. The motivation stems from our collaboration with partners who work on various materials with different types of water interaction and the methodology was adapted and applied to their materials and research questions. Several partners are found in SuMo Biomaterials, a VINN Centre of Excellence that brings together industrial and academic scientists united by a common interest in understanding the mass transport properties of supermolecular biomaterials and developing predictive models as a basis for the design of new and improved functional materials. Structure dynamics in connection to water transport has been identified as an important area of research for SuMo. However, modelling transport in systems where the structure evolves with time presents significant challenges, and experimental methods for observing such phenomena are necessary as a means of facilitating the understanding and testing predictions.

One of our collaborators is Södra Cell AB (Värö, Sweden), a company in the forestry sector that works with cellulose from wood pulp. Cellulose fibres and their wetting properties are at the heart of the pulp and paper industry, and much research is devoted to understanding the structural changes that occur in the cellulose fibre during drying and wetting processes (Laivins & Scallan, 1993; Perkins & Batchelor, 2012). The hydration and wetting properties of fibres and cellulose fibres have been studied in the ESEM previously (Jenkins & Donald, 1997; 1999; 2000; Karlsson *et al*., 1998; Wei *et al*., 2003*b*). However, these studies employed the traditional approach where *in situ* hydration is accomplished by increasing the RH through pressure increase or temperature decrease. Furthermore, to the author's knowledge, no previous attempts have been made at studying the water transport properties of individual fibres in the ESEM. As water absorption in a fibre network is a complex process with contributions from the fibre properties as well as the properties of the network structure (Karlsson *et al*., 1998), studying a cellulose fibre in isolation is important and complements previous studies with the aim of understanding the transport mechanisms involved.

We have also collaborated with the pharmaceutical company AstraZeneca (Mölndal, Sweden) on phase-separated polymer films intended as coatings for oral pharmaceutical formulations. The overall goal is to be able to tailor the mass transport properties of the coating film in order to modify the drug release from a coated drug-containing tablet or pellet. The polymer films consist of a blend of two cellulose derivatives, where one is water-soluble and can leach out when exposed to an aqueous environment. As a consequence of leaching, the permeability of the coating towards water and drug evolves with time and is largely determined by the phase-separated morphology (Marucci *et al.*, 2009). The initial wetting process has not been studied before due to a lack of available methods for studying the water transport at short time scales (of the order of seconds to a few minutes). Free films of the coating material can be used as models in order to increase the understanding of the coating properties (Frohoff-Hülsmann *et al*., 1999; Marucci *et al*., 2013). In previous studies, water transport through free films has been studied by quantitative techniques and the film microstructure has been examined separately before and after immersion in water. The understanding of the structure-transport relationships can be greatly enhanced if microstructure and local water transport can be studied simultaneously.

A third type of material was used to demonstrate additional possibilities of the new technique. The work was performed in collaboration with Dr Kristina Hedfalk in the Department of Chemistry and Molecular Biology at the University of Gothenburg whose research is focused on the structure and function of membrane proteins in cells. The cell membrane is permeable to water and the permeability is increased by the presence of membrane proteins called *aquaporins* that function as water channels. Aquaporins are crucial for the regulation of cell volume, and severe disorders and diseases can arise if their function is compromised. Therefore, the study of aquaporin function is important as a step toward the successful development of drugs that target the water transport activity of cells (Öberg & Hedfalk, 2012). When exposed to a so-called hyposmotic shock, the cell swells due to osmotic transport of water into the cell across the membrane. The role of aquaporins in cell swelling and volume regulation is not known in detail (Pasantes-Morales & Cruz-Rangel, 2010). Yeast cells have been extensively used as models to study the cell response to osmotic shock (Soveral *et al.*, 2008; Klipp, 2005). Available methods such as stopped-flow technique (Fischer *et al*.,

2009; Soveral *et al*., 2008) and optical microscopy (Soveral *et al*., 2008) have limited sensitivity and the development of complementary methods that enable the measurement of osmotic swelling in single cells with a high spatial and temporal resolution is important.

1.2 Aim of the work

The aim of this work was to enable and demonstrate new types of dynamic *in situ* experiments in the ESEM that provide novel and useful information about the water interaction of soft materials. Here, "water interaction" is used in a wide sense to include for example absorption, transport, swelling and dissolution. The work was motivated by our belief that the full potential of the ESEM in this area has not been explored. Our goal with the method development was to create a flexible platform – the *in situ* sample stage – that can be applied to different materials and types of water interaction. The work is organised into the following four papers.

In **paper I,** the aim was to develop and demonstrate an *in situ* wetting technique suitable for studies of water uptake and transport in soft materials. This required a method for controlling the point of contact between the specimen and the water and making it available for visual studies. Individual cellulose fibres were used as a model system providing a relatively simple geometry, a high capacity for water uptake and a clear visual indication of water uptake through swelling.

The aim in **paper II** was to prove the concept of a technique that can measure the time-dependent osmotic swelling of individual yeast cells in the ESEM with a high sensitivity, i.e. at a high spatial and temporal resolution. The *in situ* sample stage was coupled with a piezo-resistive atomic force microscopy (AFM) sensor to enable swelling measurement through force spectroscopy and the humidity-controlled environment of the ESEM was used to simulate a hyposmotic shock. In addition, the Young's moduli of individual yeast cells were extracted.

In **paper III**, the aim was to further develop the *in situ* ESEM technique to enable the study of film specimens with a focus on the local water transport and the correlation to the microstructure of the material. Phase-separated polymer films for controlled-release applications were chosen as model system due to their highly heterogeneous and tuneable microstructure that governs water permeability. The effect of polymer blend ratio on structure-transport relationships was studied.

Paper IV continues the theme of paper III with the wetting of phase-separated polymer films. The aim was to understand the dynamics of water interaction in the initial stage of wetting, the water transport mechanisms and the potential influence of the environmental conditions in the ESEM. The methodology was further developed to involve other arrangements of the film specimens in order to extract complementary information and allow separation of the effects of polymer swelling from those of liquid water transport. In addition, microstructural investigations in the transmission electron microscope (TEM) were performed in order to evaluate the role of porosity for the liquid water transport through the films.

2 MATERIALS STRUCTURE AND WATER INTERACTION

2.1 Cellulose fibres

The interaction between water and cellulose fibres is important in many materials-related applications, e.g. in the papermaking (Perkins & Batchelor, 2012) and wood product industries (Glass & Zelinka, 2010). This section provides a brief introduction to the structure and water interaction of cellulose fibres. The description is limited to cellulose from softwood (coniferous trees) and does not include the organisation of fibres and other structures in wood.

Softwoods consist of two different types of cells, where the largest group (90-95%) are the so-called *tracheids*. These are typically 2-4 mm long and 20-40 μm thick (Sjöström, 1993), but narrower toward the ends. The tracheids are the cellulose fibres typically used in the pulp and paper industry (Theliander *et al*., 2002), and also in the present work.

In wood, the tracheids are longitudinally oriented, i.e. along the direction of the stem or branches. They are dead cells, whose key functions are to provide mechanical support and to conduct water up the stem of the tree. A fibre consists of a cell wall with a hollow cavity, the *lumen*, running along the centre. The lumen plays an important role for the water transport through the fibre. In the wood produced during spring (*earlywood*), when the tree grows fast and requires an efficient water transportation system, the lumen is wide and the cell wall thin. Conversely, in the slow growing, denser *latewood* produced during summer, the fibres develop a thick cell wall with a narrower lumen. (Sjöström, 1993; Theliander *et al*., 2002; Rowell, 2012).

A schematic drawing of the structure of the cell wall is shown in Figure 1. It consists mainly of cellulose, hemicelluloses and lignin, and has a highly organised, hierarchical structure. Some aspects of the ultrastructure of the cell wall are still being debated and the terminology of different elements is not unified. A simplified description is given here. Cellulose molecules are arranged into bundles called *elementary fibrils* that are a few nanometres wide. These are arranged into *microfibrils* (10-20 nm wide), which are arranged into greater fibrils that form the lamellae that build up the cell wall layers known as the primary wall and the secondary wall. In the primary wall, the microfibrils are disordered but in the thicker secondary wall, they form three anisotropic lamellae where the angle of fibril arrangement varies between the layers. Between adjacent cells, there is the so-called *middle lamella* that consists mostly of lignin and holds the cells together. The warty layer is a thin, amorphous layer lining the lumen. Throughout the fibrillar structure of the cell wall, lignin and hemicelluloses are present as encrusting materials. (Côté, 1967; Sjöström 1993; Theliander *et al*., 2002; Duchesne *et al*., 2003).

Both the cell wall and the lumen interact strongly with water. The lumen acts as a channel for water transport by capillary forces due to the combination of the water-cellulose interaction and the water-air surface tension. The cell wall is a hygroscopic material, i.e. has an affinity for water, due to the hydroxyl groups present on the cellulose and hemicellulose molecules. As a consequence, the fibre will absorb moisture from the air and the moisture content will come to equilibrium with the environment according to the RH and temperature of the air (Glass & Zelinka, 2010).

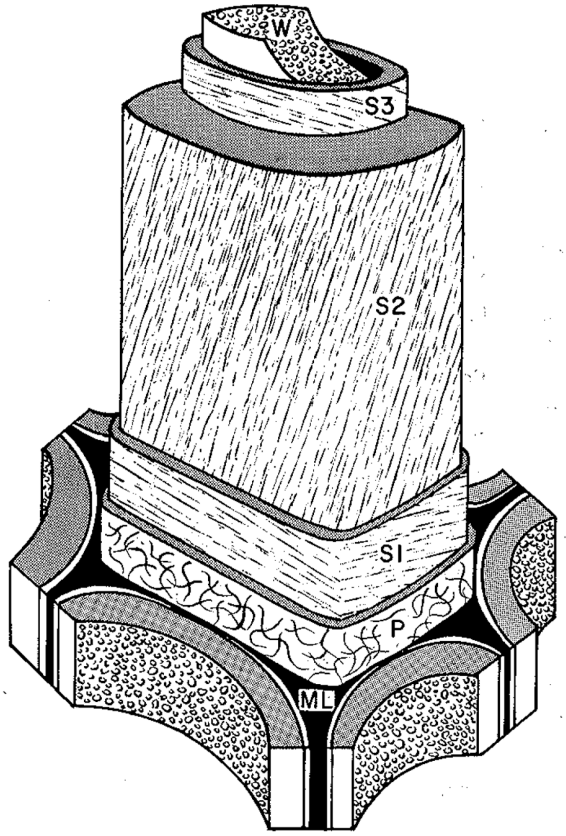

Figure 1. Schematic drawing of the cell wall layers. S1, S2 and S3 are the three lamellae of the secondary wall. P is the primary wall and ML the middle lamella. W is the *warty layer* lining the lumen. Reprinted from *Wood Ultrastructure*, A. W. Côté, ©1967, by permission of the University of Washington Press.

At the nanometre length scale, the cell wall is a porous structure and the void volume in the cell wall increases dramatically during Kraft pulping as the wood is delignified to separate the fibres. Hence, pulp fibres have a much higher porosity than native fibres (Andreasson *et al*., 2003). The pore volume in the cell wall has a large influence on the swelling properties of the fibre when exposed to water (Östlund *et al*., 2009).

Water in the cellulose fibre is often classified in terms of "bound" and "free" water (Glass & Zelinka, 2010; Perkins & Batchelor, 2012). The water in the cell wall is bound, held by intermolecular attractive forces, while the water in the lumen is considered free, i.e. not bound except by capillary forces. The so-called *fibre saturation point* (FSP) is the water content at which the fibre wall is saturated but no water exists in the lumen. This is generally around 30% (dry basis) (Glass & Zelinka, 2010), but can vary between 20% and 50% depending on tree species (Rowell, 2012). Below the FSP, the water content depends on the relative humidity and temperature of the surrounding air. The water content of the fibre can only exceed the FSP if the fibre is exposed to liquid water and all water absorbed beyond the FSP is "free" water contained in the lumen (Glass & Zelinka, 2010; Rowell, 2012). When a fibre absorbs liquid water, its water content can increase at a faster rate than possible by water vapour sorption, and the rate of absorption is highest in the longitudinal direction, i.e. in the direction of the lumen. The fibre can absorb liquid water until its maximum moisture content is reached. The maximum moisture content can be over 200% (dry basis) (Glass & Zelinka, 2010).

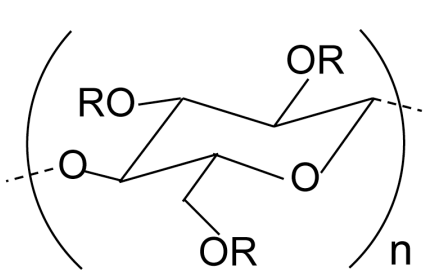

Cellulose:
R = H

Ethyl cellulose:
R = H or CH_2CH_3

Hydroxypropyl cellulose:
R = H or $CH_2CH(OH)CH_3$

Figure 2. The chemical structure of the cellulose repeat unit (unlabelled nodes are carbon atoms), including the substituent groups of ethyl cellulose and hydroxypropyl cellulose.

An important aspect of the water-fibre interaction is the process called *hornification*. It refers to changes in the structure and properties of cellulose fibres in wood pulps or paper upon drying. The pore volume in the cell wall collapses and the polymer structure stiffens. These changes are described as irreversible or partially reversible (Fernandes Diniz *et al.*, 2004), and they are manifested in the macroscopic properties of the pulp or paper. For example, the water uptake and swelling upon rewetting is diminished, and paper products suffer a loss in tensile strength (Östlund *et al.*, 2009). Hornification is thus an area of interest particularly in the pulp and paper industry, and much research is devoted to understanding the underlying mechanisms in order to be able to control the phenomenon. The hornification increases with the number of cycles of drying and rewetting. In addition, a low lignin and hemicellulose content has been shown to amplify the effects of hornification (Laivins & Scallan, 1993).

2.2 Phase-separated polymer films

The phase-separated polymer films are intended for controlled-release applications. They are based on two different cellulose derivatives: ethyl cellulose (EC) and hydroxypropyl cellulose (HPC). The chemical structures of EC and HPC are presented in Figure 2. Both EC and HPC are cellulose ethers, which means that some of the hydroxyl (OH) groups on the anhydroglucose repeat units of cellulose have been substituted by ether groups of general formula OR, where R is an alkyl group. For EC, the substituent group R is an ethyl group (CH_2CH_3); for HPC, it is a hydroxypropyl group ($CH_2CH(OH)CH_3$). The nature of the substituents and the degree of substitution control the properties of the polymer, such as solubility characteristics, degree of water uptake and glass transition temperature. The degree of substitution (DS) is the average number of substituted hydroxyl groups per anhydroglucose unit. Complete substitution would thus correspond to DS = 3 (Sakellariou & Rowe, 1995). For HPC, however, the OH group of the hydroxypropyl group can also be etherified, so that the number of moles of hydroxypropyl groups per anhydroglucose unit (the molar substitution, MS) becomes greater than 3 (Larez-V *et al.*, 1995).

Because of their chemical differences, EC and HPC interact with water in different ways. EC is not soluble in water or in the gastrointestinal tract (Sakellariou & Rowe, 1995; Lecomte *et al.*, 2003). The water permeability of EC films produced in a similar way as the EC/HPC films used in our studies (sprayed from a mixture with ethanol and a small percentage of water) is reported as 10^{-12} m^2/s (Hjärtstam & Hjertberg, 1999). HPC, on the other hand, is soluble in water at temperatures below its cloud

point, which depends on the polymer concentration but stays above 25°C (Larez-V *et al*., 1995), and in the gastrointestinal tract (Sakellariou & Rowe, 1995). In excess water, it swells without limit until the polymer molecules dissolve (Ferrero *et al.*, 2010). In concentrated aqueous solutions, a highly viscous gel-like state has been observed at a polymer concentration above 70wt% (Sudo, 2011) or volume fraction greater than 0.8 (Larez-V *et al.*, 1995). The amount of water absorbed from the vapour phase below 100% RH is usually characterised by water sorption isotherms (Chinnan & Park, 1995; Seo *et al.*, 2002; Yakimets *et al.*, 2007).

EC is widely used in pharmaceutical coatings. As it is insoluble in water, it is impermeable to most drugs and a water-soluble polymer such as HPC is often added to increase the permeability. The leaching of the soluble polymer can create water-filled pores/channels in the film (Siepmann *et al*., 2008; Harris & Ghebre-Sellassie, 2008). However, the extent of channel formation depends on the connectivity of the phase-separated morphology, which varies with the polymer blend ratio (Lindstedt *et al.*, 1991; Marucci *et al.*, 2009). When EC and HPC are co-dissolved, they phase separate as the solvent evaporates (Sakellariou & Rowe, 1986) and form domains rich in EC and domains rich in HPC. EC-rich and HPC-rich domains will henceforth be referred to simply as EC and HPC domains, respectively. Solvent evaporation increases the viscosity of the blend and the phase-separated morphology can thus be frozen before the system reaches equilibrium (Marucci *et al*., 2013a). When the volume fractions of the components are similar, phase separation can result in equal or nearly equal phase volumes (Siggia, 1979) and a bicontinuous structure can develop, where both phases are interconnected. Otherwise, the minor phase can be below a three-dimensional percolation threshold, forming discrete inclusions in the major phase (Brown and Chakrabarti, 1993). Thus, the polymer blend ratio has a large impact on the permeability of the film through its influence on the phase-separated morphology.

The microstructure of EC/HPC films has been studied by SEM (Marucci *et al*., 2009; Boissier *et al*., 2012; Andersson *et al*., 2013), NMR cryoporometry (Boissier *et al*., 2012) and confocal laser scanning microscopy (CLSM) (Marucci *et al*., 2013a). However, data on the three-dimensional microstructure is still limited. The water transport properties have been studied using quantitative techniques, mainly diffusion cells (see above-mentioned references). Marucci and co-workers (2009) found that the water permeability of EC/HPC films as well as the amount of HPC leached from the films increased dramatically when the HPC fraction exceeded 22% (w/w). They explained the critical HPC concentration as the consequence of HPC percolation in the film. Below the percolation threshold, HPC is encapsulated by EC and therefore cannot leach out; as a consequence, the film permeability is low. Above the threshold, HPC starts to form a continuous phase and a porous structure is developed upon water exposure due to leaching of HPC.

2.3 Cell wall and membrane of yeast

Yeast cells are often used as models in the study of cellular osmotic response (Klipp, 2005; Soveral *et al.*, 2008). Yeast models can increase the understanding of human cell physiology since the adaptive strategies employed by the cells are highly conserved through evolution (Somero & Yancey, 1997). A simplified schematic

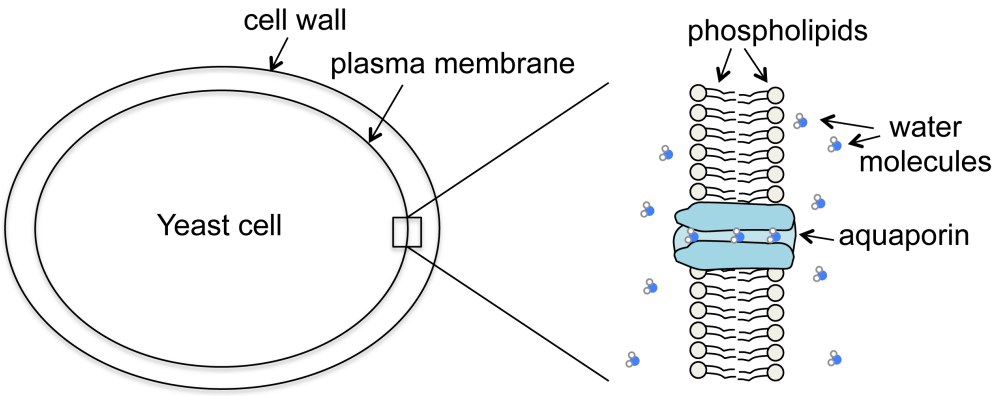

Figure 3. Simplified schematic illustration of a yeast cell. The plasma membrane and cell wall enclose the interior of the cell. The phospholipid bilayer of the plasma membrane is shown with an aquaporin (water-facilitating protein) and water molecules passing through it.

picture of a yeast cell is shown in Figure 3. The cell wall is a rigid structure that determines the shape of the cell (Blanco *et al.*, 2012) and balances the turgor pressure (intracellular overpressure) (Arfsten *et al.*, 2010) but it is also an active interface towards the environment as its composition and structure change in response to a range of environmental conditions (Smits *et al.*, 1999). It has a complex fibrous network structure composed of polysaccharides and proteins (Lipke & Ovalle, 1998). The plasma membrane is located inside the cell wall and encloses the interior of the cell. It consists of a bilayer of phospholipids with other structural components incorporated in it (Grillitsch *et al.,* 2014). The membrane is permeable to water and a net water flux into or out of the cell results in cell expansion or shrinkage, respectively. The flow of water across the membrane is driven by osmosis, where the relationship between extracellular and intracellular concentrations of solutes (osmolality) determines the direction of water flow (Verbalis, 2010). *Aquaporins* are proteins integrated in the membrane that function as channels for water and thereby increase the water permeability of the membrane (Pasantes-Morales & Cruz-Rangel, 2010; Öberg & Hedfalk, 2012).

All cells are highly dependent on the ability to maintain a constant volume, and therefore have mechanisms to regulate their volume in response to perturbations. The cell volume is governed by the amount of water in the interior of the cell, and even small changes in water content may adversely affect important processes related to cell signalling and communication as well as the integrity of functional molecules. Cell volume changes occur continuously under normal physiological conditions in response to different processes. However, pathological states of various kinds may cause more serious imbalance in osmolality (Pasantes-Morales & Cruz-Rangel, 2010). A *hyposmotic shock* is induced if the external osmolality drops rapidly. The immediate effect is a passive response of the cell in the form of swelling due to water influx. After some time, however, an active regulatory process sets in to bring the cell volume back toward normal. This process involves the export of solutes from the cell to even out the osmotic gradient and reverse the water flux (Tamás *et al.*, 2003; Verbalis, 2010). The active response, or osmoregulation, occurs more slowly than the passive response (Marechal *et al.*, 1995; Verbalis, 2010).

One place where the consequences of cell volume perturbation are particularly dramatic is in the brain. The skull is a rigid construction that restricts the brain volume and the ability of the tissue to expand is thus limited. Therefore, brain edema,

which can result from a number of different conditions including head trauma (Pasantes-Morales & Cruz-Rangel, 2010), is a serious state that can lead to neurological damage or death (Verbalis, 2010). In the brain, the aquaporin AQP4 is of particular importance for the water permeability, and studies indicate that its activity affects both the extent of cellular swelling under hyposmotic conditions and the volume regulatory response (Pasantes-Morales & Cruz-Rangel, 2010).

The yeast species used in our *in situ* ESEM studies, *Pichia pastoris*, has proven a successful host for the overproduction of the human aquaporins including AQP4 (Öberg & Hedfalk, 2012) and is therefore an interesting model species for the characterisation of aquaporins and their functions. It is possible to engineer the expression of native proteins in a strain of cells. By deleting the gene that encodes a certain membrane protein in one strain and inducing overproduction in another strain, the function of the protein can be examined through the response of the strains to external stimulus. This approach was used by Fischer and co-workers (2009) to study the water transport activity of Aqy1, which is the only aquaporin native to *P. pastoris*. They hypothesise that Aqy1 is sensitive to membrane tension (curvature), which depends on the pressure inside the cell, so that the water channel is opened and closed as a function of the pressure. Such mechanosensitive gating may protect the cell from the effects of an osmotic shock. Similarly, Soveral and co-workers (2008), who studied *S. cerevisiae* yeast cells, believe that Aqy1 is inhibited under hyposmotic shock due to development of membrane tension upon rapid cell swelling. They further speculate that this mechanism could be a first tool of the cell to decrease the water influx across the cell membrane while the mechanism for exporting solutes is being triggered, as the water channel inhibition can be expected to give a more rapid response.

3 EXPERIMENTAL TECHNIQUES

This chapter provides an overview of the basic principles of ESEM and a very brief account of the imaging mode used in the transmission electron microscope (TEM) studies of EC/HPC films. This imaging mode is called high-angle annular dark field scanning transmission electron microscopy (HAADF-STEM).

3.1 The Environmental Scanning Electron Microscope

Environmental scanning electron microscopy is a technique used to investigate the microstructure of materials in a controlled sample environment. This section provides an overview of the basic principles of the ESEM with a focus on experiments involving water. The description is based on the works by Stokes (2008) and Donald and co-workers (2000), where extensive information about the technique can be found. Examples of applications of the ESEM and current *in situ* methods were given in the introductory chapter of the thesis.

In a conventional SEM, high vacuum is maintained throughout the electron-optics column and the sample chamber in order to prevent scattering of the electron beam. To comply with the high vacuum requirement, specimens must not contain any volatile substances, such as e.g. water or oil. Also, they need to be electrically conducting or they will accumulate negative charge during imaging with electrons, resulting in adverse effects on the image quality. These constraints limit the possibilities of examining certain types of materials with SEM, for example many biological materials and food substances as well as most polymers. Water can be removed from a specimen by freeze-drying, for example, and electrically insulating materials can be coated with a conducting layer to reduce charging. However, these types of sample preparation may change the structure of the material, obscure fine detail or introduce other artefacts, possibly leading to misinterpretation of images. Moreover, applying a coating can limit the possibilities of obtaining compositional contrast from the material and of performing dynamic experiments *in situ.*

The ESEM circumvents the limitations and offers greater freedom in terms of the types of materials that can be imaged as well as the design of experiments. The essential difference between a conventional SEM and an ESEM is the ability of the latter to operate with a gas in the sample chamber, typically at pressures of up to 20 torr. The microscope is equipped with a series of pressure-limiting apertures (PLA) and a differential pumping system that limit the amount of gas in different sections of the electron-optics column and keep the upper section, where the electron source resides, at high vacuum. The gaseous secondary electron detector (GSED), which acts as the final PLA, has a positive bias that attracts the secondary electrons emitted by the specimen.

The gas plays an active role by enabling signal amplification through ionising collisions with the electrons. The resulting cascade of electrons are accelerated towards the detector, and the positive ions left in the gas drift to the specimen surface where they recombine with free electrons to prevent the build up of static charge in the material. This process, illustrated in Figure 4, makes it possible to image insulating specimens without applying a conductive coating. In order to limit the scattering of the primary electron beam in the gas, it is important to maintain a small working distance at high gas pressures. A number of different gases can be used and

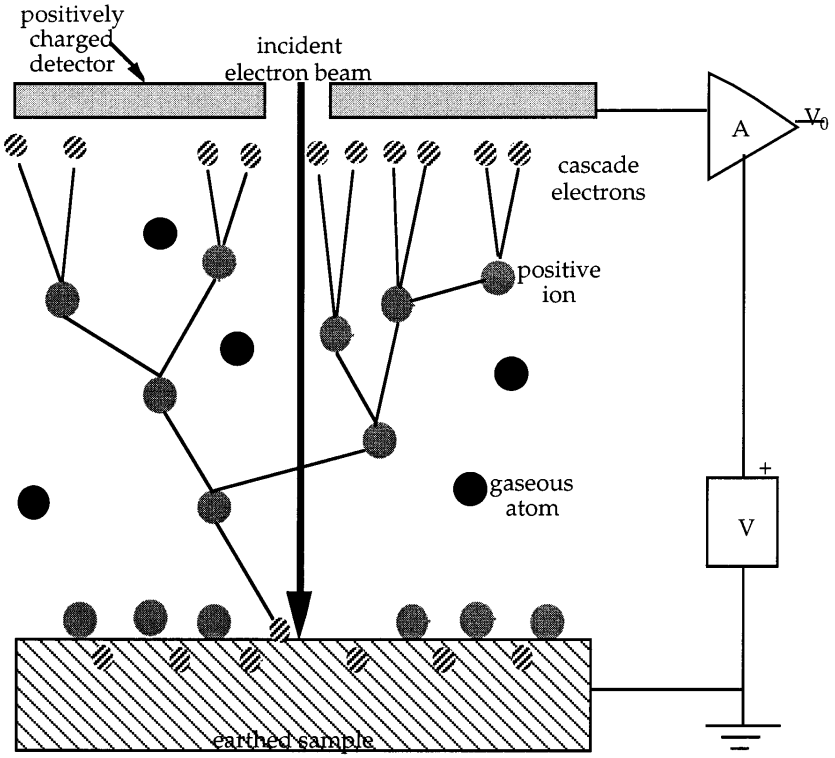

Figure 4. Schematic representation of the cascade amplification process in an ESEM. An electron leaving the sample surface collides with gas atoms/molecules to create a cascade of electrons that amplify the signal (electron trajectories illustrated by lines). Positive ions resulting from the collisions drift toward the sample surface where they recombine with electrons on the surface. Reprinted from Colloids and Surfaces A, 174, pp. 37-53, A. M. Donald, C. He, C. P. Royall, M. Sferrazza, N. A. Stelmashenko and B. L. Thiel, © 2000, with permission from Elsevier.

the choice depends on the material under study as well as the purpose of the investigation. Water vapour constitutes a special case where, in addition to signal amplification, the gas can also be used to stabilise the water content in moist specimens and even perform dynamic experiments involving the hydration or dehydration of materials *in situ*.

In order to control the state of hydration of a sample, both its temperature and the water vapour pressure in the surrounding environment must be controlled as they determine the RH at the sample site. The saturated vapour pressure (SVP) curve, depicted in Figure 5, is part of the phase diagram for pure water and maps out the points of thermodynamic equilibrium between the liquid and gas phases. It can be used to determine the combination of pressure and temperature needed to balance condensation onto and evaporation from the specimen in order to stabilise its moisture content in the microscope chamber. However, for specimens that contain aqueous phases with dissolved solutes such as e.g. salts or different biomolecules, the curve is downshifted to account for the water activity of the sample. If a specimen has water activity a_w, the equilibrium vapour pressure p_{eq} can be related to the SVP of pure water p_0 at the same temperature by

$$p_{eq} = a_w p_0$$

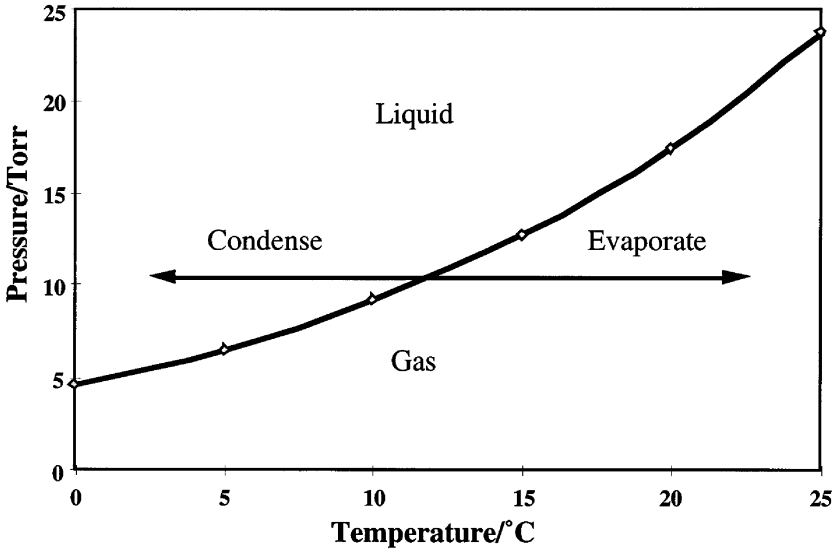

Figure 5. The saturated vapour pressure curve for water. Reprinted from Colloids and Surfaces A, 174, pp. 37-53, A. M. Donald, C. He, C. P. Royall, M. Sferrazza, N. A. Stelmashenko and B. L. Thiel, © 2000, with permission from Elsevier.

and the relative humidity can be expressed as $RH = a_w \cdot 100$. Condensation or evaporation will occur in the non-equilibrium regimes above or below the SVP curve, respectively. This can be used to hydrate or dehydrate the specimen *in situ*, while the dynamics of the process are being followed in real time through imaging. Thus, certain properties of the material under study can be directly related to its microstructure.

Before microscopy can begin, the pressure inside the sample chamber must be brought down to operating pressure and the air must be replaced with water vapour. For moist specimens sensitive to dehydration, this is an important step. Purge-flood cycles can be employed to successively exchange air for water vapour. In addition, a few droplets of water can be placed at a non-cooled area close to the specimen in order to boost the water vapour pressure through evaporation during pump-down.

The microscope used throughout our experimental work was an FEI Quanta 200 FEG ESEM (FEI Company, Hillsboro, OR, USA). Additional equipment consisted of a Peltier cooling stage capable of operating in a temperature range of -25°C to 55°C, as well as the *in situ* sample stage developed in this work and its electronic control equipment. For details concerning imaging parameters and environmental conditions, see sections 4.2 through 4.4.

3.2 High-angle annular dark field scanning transmission electron microscopy

In the TEM, the microstructure of thin specimens (often thinner than 100 nm) can be investigated by using electrons transmitted through the specimen to form an image of the specimen. The electron beam can be laterally raster scanned as a sharp probe across the specimen in a scanning transmission electron microscopy (STEM) mode. Different imaging modes can be used, and one mode is called high-angle annular dark field (HAADF) STEM. In HAADF-STEM, electrons that have undergone incoherent scattering (Rutherford scattering) by the atomic nuclei in the material are used to form an image and the type of contrast created is known as mass-thickness contrast. The

cross-section for Rutherford scattering is a function of the atomic number *Z*. The higher the *Z*, the greater is the fraction of electrons that are scattered to high angles. The detector is placed in a focal plane and the camera length is used to control the collection angle interval. An HAADF detector uses high angles to avoid contributions from Bragg scattering for crystalline specimens. (Williams & Carter, 2009).

The contrast observed in an HAADF image can be caused by a variation in mass, density and/or thickness. The higher the thickness, density or atomic number, the higher is the intensity in the image. (Williams & Carter, 2009).

The HAADF-STEM analysis was performed on an FEI Tecnai T20 TEM (FEI, USA) with a LaB_6 electron source, at an electron acceleration voltage of 200 kV.

4 DEVELOPMENT OF *IN SITU* ESEM METHODS

The goal in developing new methods for *in situ* ESEM studies was to create a versatile experimental platform that can be used for several different types of studies of soft materials and their interaction with water. Two main applications inspired the design of the platform, namely the wetting of materials in different shapes and orientations with focus on liquid water transport, and the real-time measurement of the swelling of hydrated materials with high spatial and temporal resolution. The developed platform, which we shall call the *in situ* sample stage, is designed for use with the FEI Quanta 200 FEG ESEM. It consists mainly of a nanomanipulation system, a design for local cooling of a site readily accessible to the nanomanipulator and a fixture to make the setup compatible with the Peltier cooling stage in the ESEM. For *in situ* measurements of swelling through force spectroscopy, a piezoresistive AFM sensor was coupled to the nanomanipulation system, enabling the measurement of forces in the nanoNewton range. The force reading can be converted to sensor tip displacement using the spring constant of the AFM cantilever.

An acceleration voltage of 5 kV was used for imaging of all materials.

4.1 The *in situ* sample stage

Figure 6 shows photos of the *in situ* sample stage in its two configurations: for wetting in (a) and for force measurements in (b). With reference to the numbers in the images, the main parts are

1. Aluminium (Al) fixture
2. Nanomanipulator
3. Copper (Cu) cylinder
4. Al wire as specimen holder
5. AFM sensor

These parts will be described in greater detail in the following sections. In addition, an external pressure gauge connected to the microscope sample chamber was used for recording pressure variations during the measurements on yeast cells, but will not be described further.

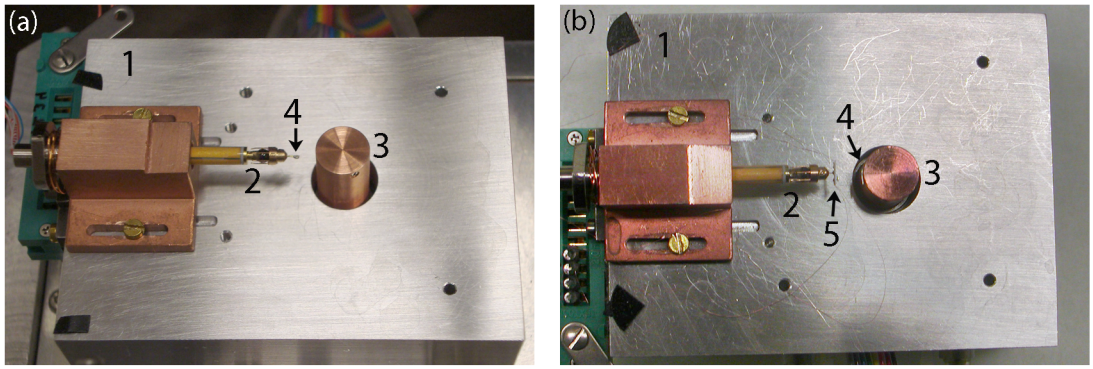

Figure 6. Photos of the *in situ* sample stage in its two configurations: (a) for wetting, and (b) for force measurements. See text for number references.

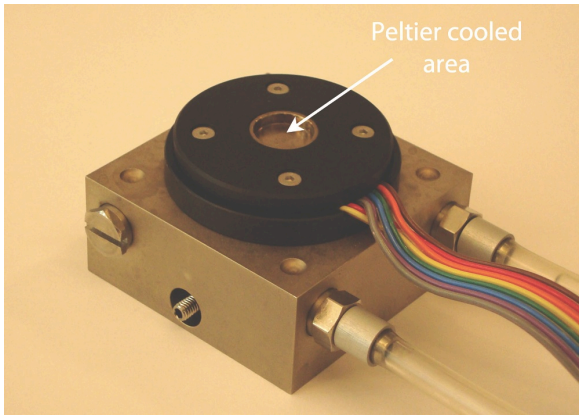

Figure 7. The Peltier cooling stage of the FEI Quanta 200 FEG ESEM, with the cooled area highlighted.

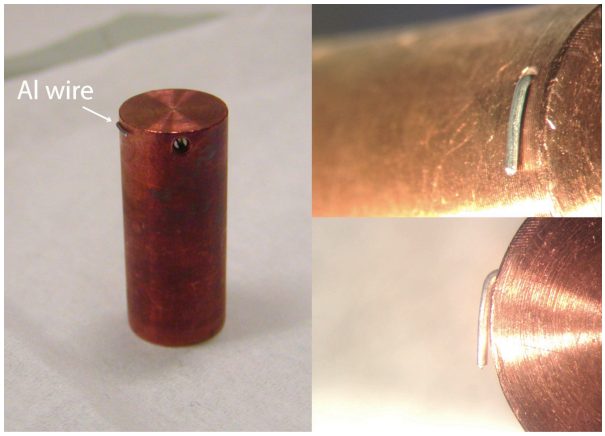

Figure 8. The Al wire used as a substrate for the cells is shown protruding from the Cu cylinder. Insets to the right show the arrangement from different angles.

There is another important part of the instrumentation that is not visible in Figure 6, namely the Peltier cooling stage shown in Figure 7. In both configurations, the Al fixture is clamped on top of the cooling stage and the Cu cylinder is placed in contact with the Peltier-cooled area of the cooling stage through an opening in the fixture. By design, the thermal contact between the cooling stage and the fixture is poor. Consequently, the Cu cylinder is the only part that is actively cooled and the rest of the setup remains closer to room temperature. This is important for two reasons: (1) to be able to maintain a water reservoir on the cylinder during *in situ* wetting while the specimen remains relatively dry prior to contact with the liquid water, and (2) to avoid excessive thermal loading of the Peltier element.

The position of the specimen is not the same in the two configurations of the *in situ* sample stage. In the wetting experiments, the specimen is glued to an Al wire mounted on the nanomanipulator. For the force measurements, the nanomanipulator is instead occupied by the AFM sensor, which is used to probe the specimen. The specimen is located on the Cu cylinder. It is actively cooled in order to be able to control the RH at the specimen site. For the yeast cells, an Al wire (0.3 mm diameter) protruding from the cylinder was used as a sample holder because (1) the cells showed a greater tendency for attachment on the Al surface than on the Cu surface and (2) the curvature of the wire surface increased the possibility of successfully contacting a single cell with the sensor tip. The arrangement is shown in Figure 8.

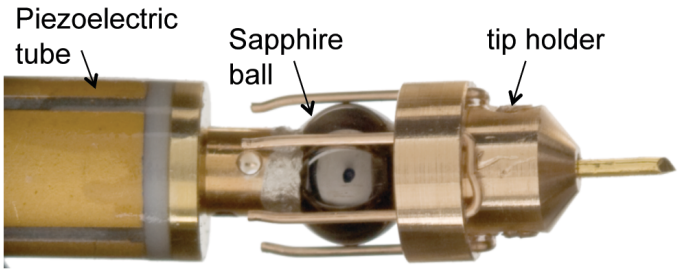

Figure 9. The nanomanipulator with its main parts: the piezoelectric tube, the sapphire ball and the movable tip holder.

The wire was inserted into a slot in the cylinder, fastened with a screw and bent to the side to become almost parallel to the vertical Cu wall.

4.1.1 Nanomanipulator

The nanomanipulator, shown in Figure 9, is a key constituent of the *in situ* sample stage. It has been developed and produced by Nanofactory Instruments AB (Gothenburg, Sweden) and has a compact design as it was originally built for use inside the TEM. The main parts of the nanomanipulator are (Svensson *et al.*, 2003):

- a piezoelectric tube with four electrodes on its surface
- a sapphire ball attached rigidly to the piezo tube
- a movable part with six springy legs gripping the sapphire ball

The movable part holds a tip where a sample (or the AFM sensor) can be placed and will henceforth be referred to as the *tip holder*. The same type of Al wire used as a sample holder for the cells was used as the tip.

This setup enables both coarse and fine movement in three dimensions. The coarse movement is accomplished through inertial sliding of the tip holder against the sapphire ball when applying short voltage pulses to the piezo tube in rapid succession. This mechanism is capable of steps down to 0.1 µm and the stepping speed is tuneable. With a total range of approximately 1 mm it is very useful for aligning the tip against a selected feature during experiments. The expansion and contraction of the piezoelectric tube with applied voltage can be used to fine-tune the alignment on the nanometre length scale. For details, the reader is referred to Svensson and co-workers (2003).

4.1.2 Aluminium fixture

Part of the development work was to design a fixture that could make the rest of the instrumentation compatible with the Peltier cooling stage of the microscope. There were several design requirements to take into account. The fixture should accommodate the nanomanipulator and its housing. Electrical connections for the signal input and output also had to be fitted on the fixture, with further connections to a feed-through flange in the microscope chamber wall. The fixture should also provide access to the cooled area of the cooling stage underneath it. It should be easy to fit over the cooling stage, yet thermally insulated from it to avoid excessive thermal

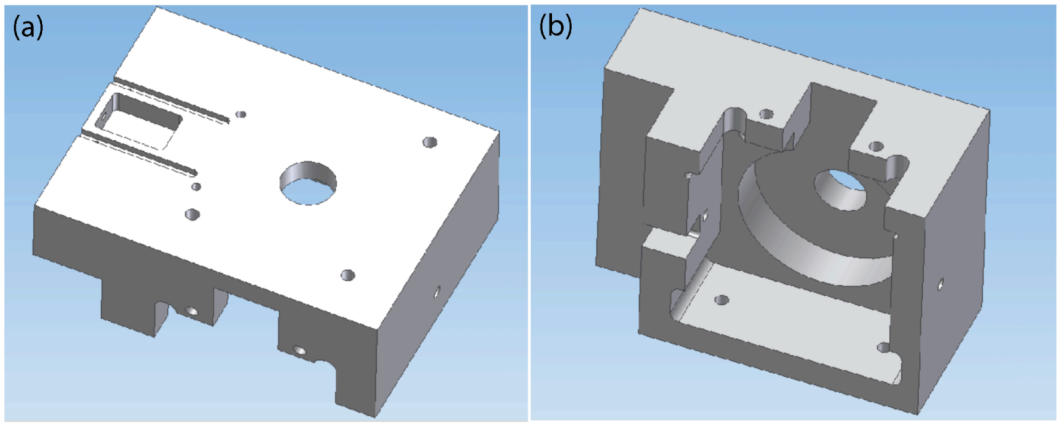

Figure 10. CAD drawing of the Al fixture, viewed from the top (a) and from the bottom (b). The shape is designed to fit over the Peltier cooling stage shown in Figure 7, and the central opening provides access to the Peltier-cooled area of the cooling stage.

loading of the Peltier element. Ultimately, all of this must be accomplished in the restricted space inside the microscope chamber.

The resulting design is shown in the form of a CAD drawing of the fixture in Figure 10. The depression on the left part of the fixture in (a) is where the nanomanipulator is installed. The position of the nanomanipulator can be adjusted along the two parallel grooves. The bottom view in (b) shows that the fixture is tailored to fit the shape of the cooling stage. The fixture is locked into place by nylon screws that create an air gap between the two parts, preventing heat conduction from the fixture to the cooling stage. The hole in the centre provides an opening for accessing the Peltier-cooled area. Electrical connections are not included in the figure.

4.1.3 Copper cylinder

As explained above, the *in situ* sample stage has two configurations to enable wetting experiments and force measurements related to the swelling of hydrated materials. Both types of experiment require local cooling of a site readily accessible to the nanomanipulator. To this end, we used a cylindrical block of solid Cu with a high purity for optimal heat conductance. The Cu cylinder was shown in Figure 8. It had a height of approximately 20 mm to match the height of the nanomanipulator and a diameter of 9.5 mm corresponding to the size of the Peltier-cooled area on the cooling stage. This provided sufficient heat conductance and a simple geometry that fits the demands of the applications.

An important aspect is the thermal equilibration throughout the Cu cylinder. In paper I, it was found that the temperature at the top of the cylinder was equal to that at the bottom after a few minutes, indicating thermal equilibration. In practice, at least 10-15 min elapsed before the *in situ* experiment began. For the yeast experiments, the temperature at the surface of the Al wire used as a sample holder was approximately 2°C when the temperature of the cylinder was set to 1°C. This may be explained by either the small contact area between Al and Cu inside the slot in the cylinder, thermal contact resistance at the interface, the comparatively poor heat conductivity of Al, the fact that the wire was protruding from the cold cylinder or a combination of these. It is important to be aware of the discrepancy in temperature when calculating the RH at the sample site.

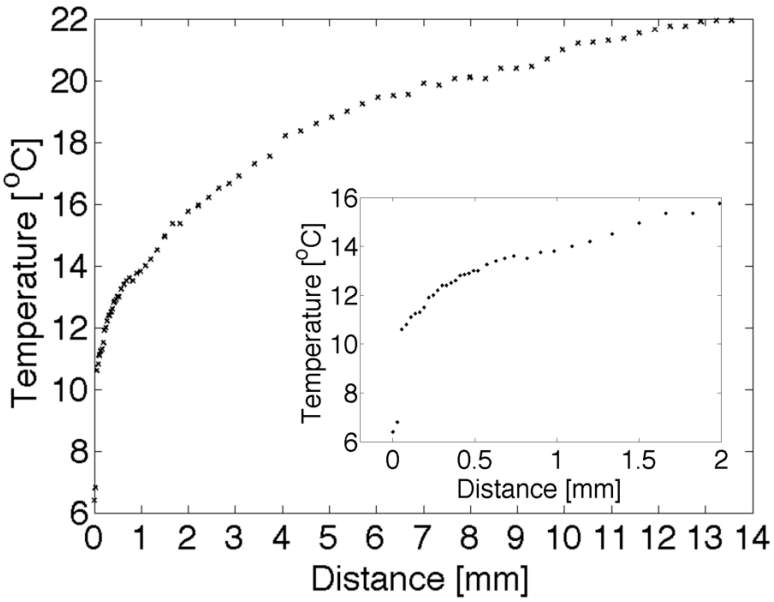

Figure 11. The temperature as a function of radial distance to the vertical wall of the Cu cylinder, measured with a type K thermocouple. The cylinder was kept at 1°C. The inset is a close-up of the region closest to the cylinder.

For the *in situ* wetting experiments, it is also important to be aware of the temperature gradient that prevails in the vicinity of the cold Cu cylinder. The temperature was measured as a function of radial distance from the vertical wall of the cylinder using a type K thermocouple. The measurement was made close to the top of the cylinder, with the thermocouple arrangement similar to the specimen arrangement in Figure 12(c). The temperature of the cylinder was kept at 1°C and the pressure at 4.93 torr. Figure 11 displays the result. The temperature decreases as the cylinder is approached and the gradient steepens. The temperature measured at contact was approximately 6°C. It differs from the expected 1°C, probably due to the very small contact area between the surface of the spherical thermocouple junction and the wall of the cylinder. The knowledge about the gradient in temperature, and hence in RH, is important in papers I, III and IV.

4.1.4 AFM sensor

The AFM sensor used in the experiments was developed and characterised by Nafari and co-workers (2008), and has an on-chip integrated Wheatstone bridge for piezoresistive force transduction. This microelectromechanical system (MEMS) sensor features a cantilever with a pyramidal tip for probing the specimen. The bandwidth of the electronics is 5 kHz to enable recording of events on the millisecond time scale. The AFM sensor was provided by NanoFactory Instruments AB and the value of the spring constant of the cantilever was given by the manufacturer as 2.8 N/m. To integrate the sensor with the *in situ* sample stage, the printed circuit board of the sensor was glued to an Al wire that fitted into the tip holder of the nanomanipulator. To transfer the signal from the sensor to the read-out electronics, four Cu wires with a thickness of 50 μm were soldered to the backside of the sensor's printed circuit board and led to a terminal of electrical contacts on the side of the Al fixture. The wires had to be thin and long enough not to obstruct the movement of the tip holder during operation of the nanomanipulator.

The output from the AFM sensor is a voltage that is translated directly in the control software into a force using known parameters for the spring constant of the cantilever and the electrical sensitivity of the sensor (Nafari, 2010). Two different types of force measurements can be performed. The first is simply a log of the force registered by the sensor over time. This was used to measure the displacement of the sensor tip in contact with individual yeast cells as a result of increased RH in paper II, providing a measure of the cell size change. The other type of measurement is a force-displacement curve produced by the sensor approaching and then retracting from the specimen, thus loading and unloading the cantilever. This method was used to probe the Young's modulus of the yeast cells in paper II.

4.2 *In situ* wetting

During an *in situ* wetting experiment, the specimen goes from relatively dry to wet and the processes involved, for example microstructure evolution and liquid water transport, are imaged. The specimen is situated on the tip of an Al wire mounted on the tip holder. On the vertical wall and horizontal top surface of the cooled Cu cylinder are water droplets acting as reservoirs for wetting of the specimen. Figure 12 illustrates the working principle, where the manipulator is used to bring a specimen in contact with a water droplet. The setup is flexible with respect to specimen shape and orientation. The orientations in (a) and (b) for film specimens will be referred to as surface mode and cross-section mode, respectively. In (b) and (c), the point of contact between the specimen and the water is visible. In surface mode (a), the point of contact is not visible but an instantaneous saturation of the GSED upon contact can conveniently be used as an indicator of the time of contact. The saturation occurs due to sudden evaporation of liquid water from the reservoir upon contact with the non-cooled specimen, as indicated by control experiments without a water reservoir. Following saturation, readjustment of the brightness and contrast is necessary in order to quickly restore the image. Also, the focus sometimes needs slight adjustment due to movement of the specimen in the downward direction upon contact in surface mode.

The positioning of the specimen can be accurately controlled using the manipulator. When the water reservoir is visible, as in Figure 12 (b) and (c), alignment with the water reservoir in the direction of the electron beam is accomplished by bringing both objects into focus at the same time. In surface mode, a gradual and sufficiently slow approach makes it possible to maintain focus through the approach in the downward direction toward the reservoir. In the performed wetting experiments, the tip holder always constituted the highest point of the setup. The working distance from the pole piece to the specimen surface was kept greater than about 5 mm (which can be less than 5 mm from the PLA of the GSED) without risk of the tip holder crashing into the detector. In order to maintain a sufficient signal-to-noise ratio, the working distance was kept smaller than about 7 mm.

Preparatory steps needed before an *in situ* wetting experiment can begin includes setting the temperature of the Peltier cooling stage and allowing sufficient time for temperature equilibration throughout the Cu cylinder as described above in section 4.1.3, mounting the tip holder with the specimen and performing a coarse alignment of the specimen with respect to the Cu cylinder. The coarse alignment can be accomplished by moving the housing of the manipulator until the specimen is at a suitable distance from the cylinder. A distance of 1-2 mm was suitable in the

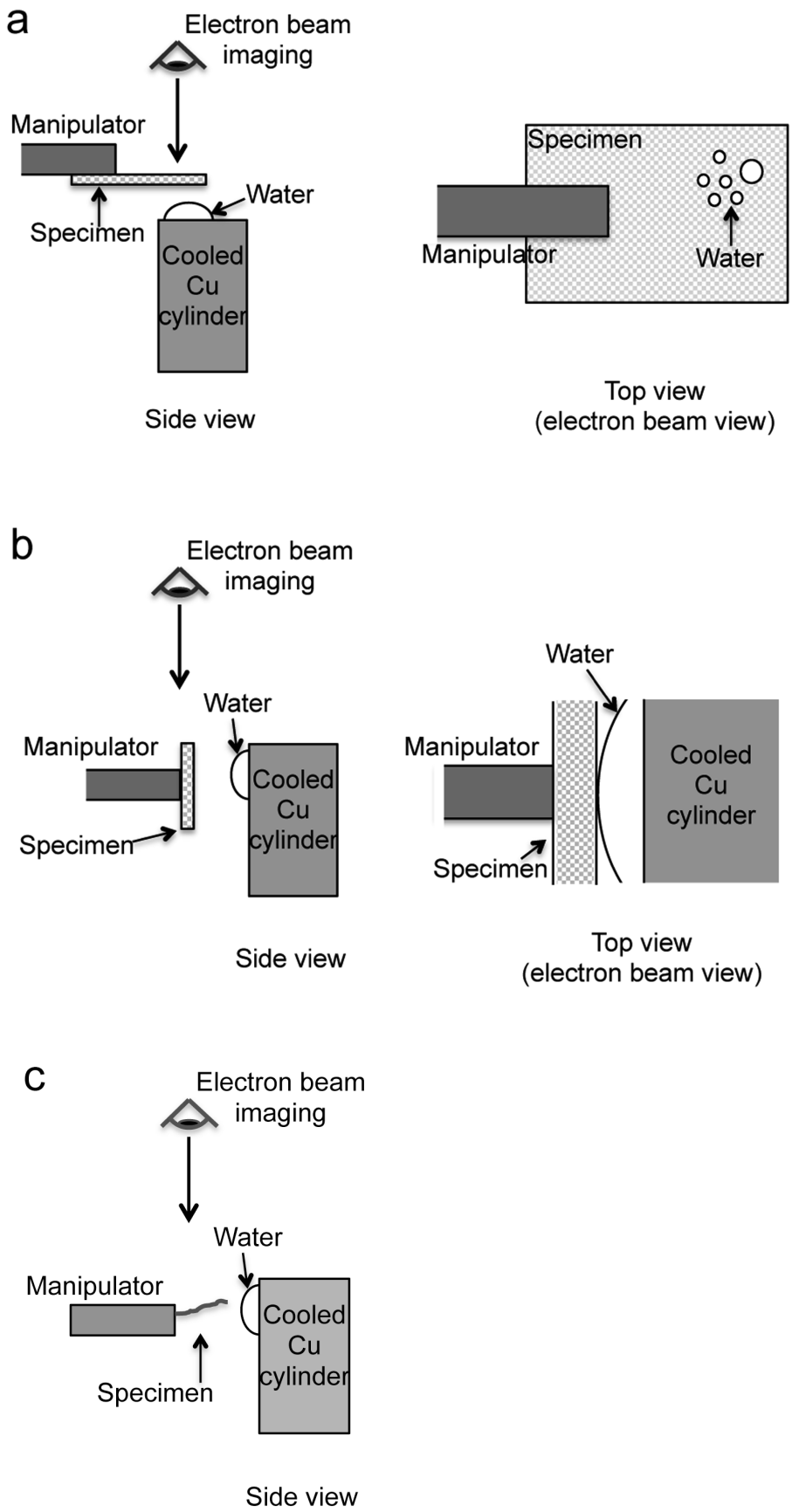

Figure 12. Schematic drawing of the setup used for *in situ* wetting of film specimens in surface mode (a) and cross-section mode (b) and of fibre specimens (c).

experiments with regard to the range of movement of the manipulator and the "thickness" of water reservoirs on the cylinder. Based on the temperature data presented in Figure 11 and the SVP curve for pure water in Figure 5, the RH is estimated to roughly 30-40% at this distance when the temperature of the Peltier cooling stage is 1°C and at the pressures used in the wetting experiments.

The microscope chamber was pumped to operating pressures using a built-in protocol that gradually exchanges air for water vapour without purging the microscope chamber (Dufek & Hayles, 2003). The starting operating water vapour pressure was chosen differently for cellulose fibres and polymer films but was always lower than the condensation pressure; the details are found in the respective papers. At 1°C condensation occurs at a pressure of 4.93 torr according to the SVP curve for pure water. However, the exact condensation pressure on the top of the Cu cylinder was measured independently for the cellulose fibre study and for the studies on polymer films, with the temperature of the Peltier element set to 1°C. During the time that passed between those studies, the condensation pressure increased slightly but was always rather consistent during the experiments of a study and corresponded to a temperature between 1°C and 2°C on the top of the cylinder. Thus, the condensation pressure was 4.93 torr in the cellulose fibre study (paper I), 5.08 torr in the first polymer film study (paper III) and 5.17 in the second polymer film study (paper IV). The reason for the change in condensation pressure over time is unclear. Possible reasons include a difference in cleanliness of the Cu cylinder or a suboptimal contact between the cylinder and the Peltier-cooled surface, although the cylinder was cleaned and the contact checked at each experiment.

Water droplets were formed on the cooled Cu cylinder by increasing the water vapour pressure above the condensation point. After a certain time, the pressure was gradually lowered to the condensation point to stabilise the droplets. The exact procedure is described in more detail in each of the papers. In the case of the polymer films, a pressure slightly higher than the condensation pressure (5.10 torr in paper III and 5.20 torr in paper IV) was required in order to stabilise the condensed water when a polymer film was present in the vicinity of the reservoir. A possible explanation is a slight elevation of the temperature of the surface water. The size of the water droplet used as a reservoir for wetting can be controlled to an extent through the choice of droplet, but also through the water vapour pressure. The pressure can be used to induce a general growth or shrinkage of the droplets at any time and then gradually restored to the desired operating pressure. However, at the later stages of approach when the specimen is close to the Cu cylinder, caution should be taken with regard to such adjustments in order to keep the moisture content of the specimen stable. It is useful to take a few images of the specimen before and after a period of elevated pressure to be able to spot any differences in the appearance due to the change in relative humidity.

In some experiments with the phase-separated polymer films (paper III), the pressure was lowered to 4.5 torr after the sample had been in contact with the water for an extended period of time in order to induce evaporation of the water on the film surface. The purpose was to investigate the occurrence of residues from the droplets of HPC solution on the surface.

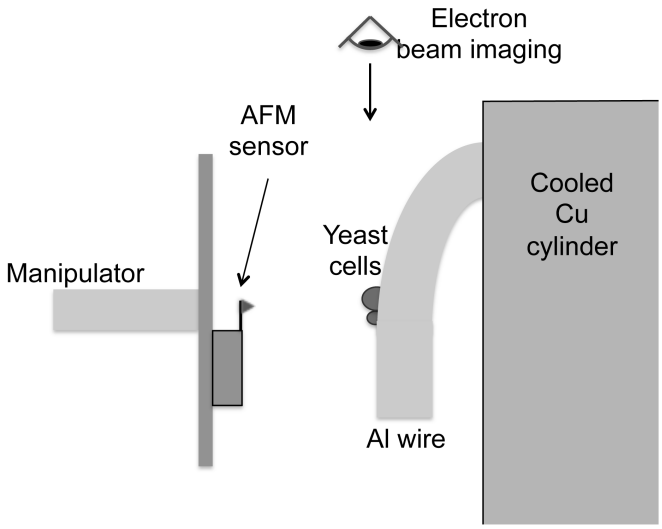

Figure 13. Schematic drawing of the setup used for measuring the osmotic response of single yeast cells in the ESEM. Depending on the specimen geometry and imaging considerations, a configuration where the Al wire is bent along the perimeter of the cylinder can also be used.

The wetting process was captured by recording movies and images. The electron beam scanning speed varied during the experiments and a faster scan was used for movie recording than for recording still images in order to capture the dynamics of processes. However, as there is a trade-off between scanning speed and signal-to-noise ratio, movies were typically recorded with a frame time of 1 s or greater to maintain an acceptable signal-to-noise ratio. Estimates of the maximum electron dose during *in situ* wetting are provided in papers III and IV.

4.3 *In situ* force measurement for swelling

As mentioned in section 4.1.4, we can perform two different types of measurement using the AFM sensor. For yeast cells, this was explored to obtain (1) the cell expansion due to osmotic shock in the ESEM, and (2) the Young's modulus of cells at 66% RH. The first of these methods is described here and the second in section 1.1.1. The descriptions are specific for the yeast experiments but the approach can be extended for the characterisation of swelling and Young's modulus in other soft materials.

The setup used for *in situ* measurements of cell expansion is schematically illustrated in Figure 13. The AFM sensor tip was placed in contact with a yeast cell. In order to induce cell expansion, the water vapour pressure in the sample chamber was increased. This increased the water potential outside the cell and created a situation analogous to a hyposmotic shock, i.e. a net influx of water into the cell across the cell membrane. The resulting displacement of the sensor tip, corresponding to the change in size of the cell, was measured with high spatial and temporal resolution by recording the time-dependent cantilever deflection.

The preparations were carried out as follows. The AFM sensor was mounted on the tip holder of the manipulator and its electrical contacts were connected to the control system. The Cu cylinder, with the Al wire containing the adsorbed yeast cells, was put in place on the *in situ* sample stage in contact with the Peltier-cooled surface. The Peltier cooling stage had been precooled to 1°C and, as mentioned in section 4.1.3, a

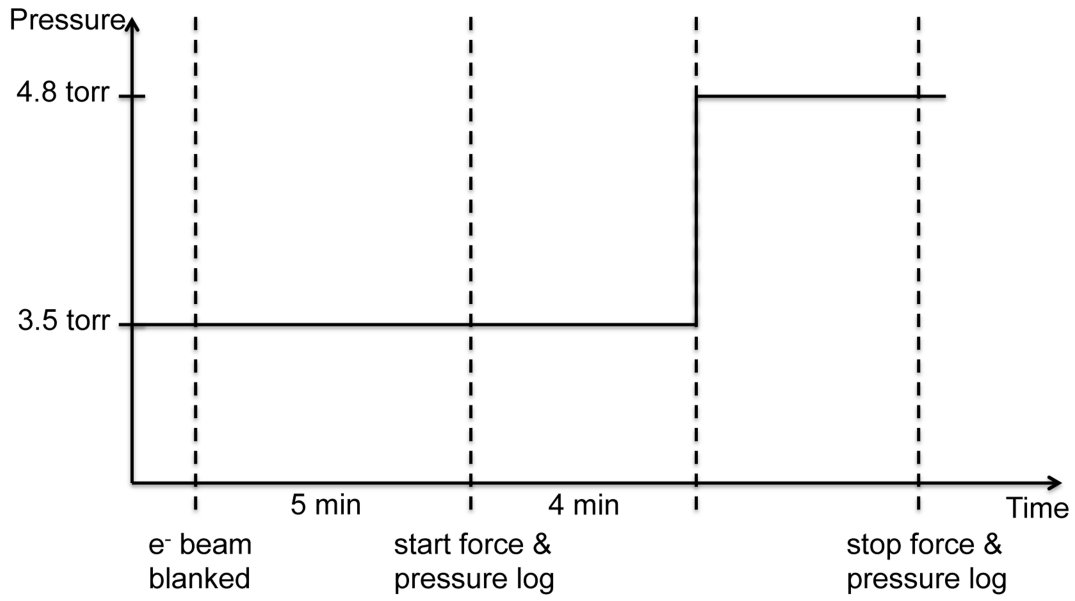

Figure 14. Schematic representation of protocol for pressure change used for the experiments on yeast cells in the ESEM. Specific events are marked along the time axis.

few minutes of equilibration time had shown to bring the temperature at the specimen site (i.e. the Al wire) to 2°C. A coarse alignment of the sensor cantilever and the sample was made. The preparations were performed as quickly as possible to minimise the exposure of the sample to the environmental conditions of the lab.

A few water droplets were placed on the surface of the Al fixture around the Cu cylinder and the pressure in the microscope chamber was brought to 3.5 torr using the same gradual pump-down sequence as in the wetting experiments (section 4.2). The relative humidity at 2°C and 3.5 torr is 66%. After initiation of imaging at an acceleration voltage of 5 kV and a working distance of 5-6 mm, the manipulator was used to bring the sensor tip into contact with a suitably located yeast cell on the Al wire. Alignment in the direction of the electron beam was performed by focusing on the yeast cell and adjusting the height of the cantilever tip until the tip apex came into focus. The alignment procedure was performed at relatively low magnification as far as possible in order to minimise the electron dose of the cell. Also, the beam was blanked at times when imaging was not needed.

Before the measurement, the electron beam was blanked to allow stabilisation of the AFM sensor in the absence of interference with the beam. After 5 minutes, the force reading from the sensor had stabilised and logging of the force output was started. At the same time, logging of the pressure in the microscope chamber was started. The pressure was measured by a pressure gauge connected to the sample chamber and recorded using an oscilloscope. After a baseline of 4 minutes had been acquired, the pressure was increased to 4.8 torr, which at 2°C corresponds to 90% RH. The force and pressure logging continued for another few minutes until the force reading appeared to have stabilised. A schematic representation of the experiment is shown in Figure 14.

The same experiment was performed on the surface of the Al wire, i.e. the substrate at which the yeast cells were located, soon after the measurement on the yeast cell was completed. The purpose was to obtain a reference curve that would be subtracted

from the yeast cell curve in subsequent data analysis, to compensate for movement of the substrate in connection to the pressure change. Such movements could be the result of e.g. thermal expansion of the Cu cylinder and/or Al wire due to increased impingement of water molecules upon pressure increase. The reference measurement was performed in close proximity to the chosen yeast cell, with the sensor tip contacting the surface of the Al substrate.

The cell expansion due to osmotic shock was obtained from the force measured by the AFM sensor during the pressure change experiment. The force was transformed to displacement of the AFM tip using the spring constant of the cantilever. The temporal correlation of the cell expansion curve with the pressure curve was sorted out using time stamps contained in the raw data files.

The viability of the cells in the ESEM environment was assessed at an early stage. The tests indicated a survival rate of about 95% after 90 min at 75% RH, and 60% at 50% RH. The *in situ* experiments were performed at 66%-90% RH and within 90 min. Viability results from previous reports vary, where some indicate a more negative impact of the ESEM environment compared to our results (Ren *et al.*, 2008) while others show that yeast cells may survive at RH as low as 40% (Shen *et al.*, 2011). The differences between the results of viability tests may stem from a number of aspects, e.g. the sample preparation and handling or the pump-down procedure used. Moreover, no signs of radiation damage of cells were observed in our studies. Yeast cells have been imaged at 5 kV in the ESEM before without noticeable specimen degradation (Goponenko *et al*., 2011). Ahmad and co-workers (2008; 2010) used an accelereation voltage as high as 15 kV.

4.4 Complementary *in situ* methods

In addition to *in situ* wetting and *in situ* force measurement for swelling, complementary *in situ* ESEM methods were used.

4.4.1 In situ *vapour sorption*

For the polymer films in paper IV, experiments involving hydration through water vapour sorption were performed in addition to the *in situ* wetting experiments. Similar to the traditional way of hydrating a specimen in the ESEM, the sample was actively cooled by the Peltier cooling stage and the RH at the sample site was increased by increasing the water vapour pressure in the sample chamber.

The setup for *in situ* vapour sorption is shown schematically in Figure 15. This simpler setup does not involve the Al fixture and the manipulator but simply consists of the Peltier cooling stage and a sample holder in the form of an Al cylinder. The Al cylinder is the standard sample holder delivered with the Peltier cooling stage; it has the same diameter as the Cu cylinder but only a fourth of its height, as the Cu cylinder was designed to match the level of the specimen attached to the manipulator. In the absence of the fixture and manipulator, we chose to use the Al cylinder as the Cu cylinder would have exposed a relatively large surface area for water molecule impingement from the surrounding gas. The protocol used for pressure increase is shown in Figure 16.

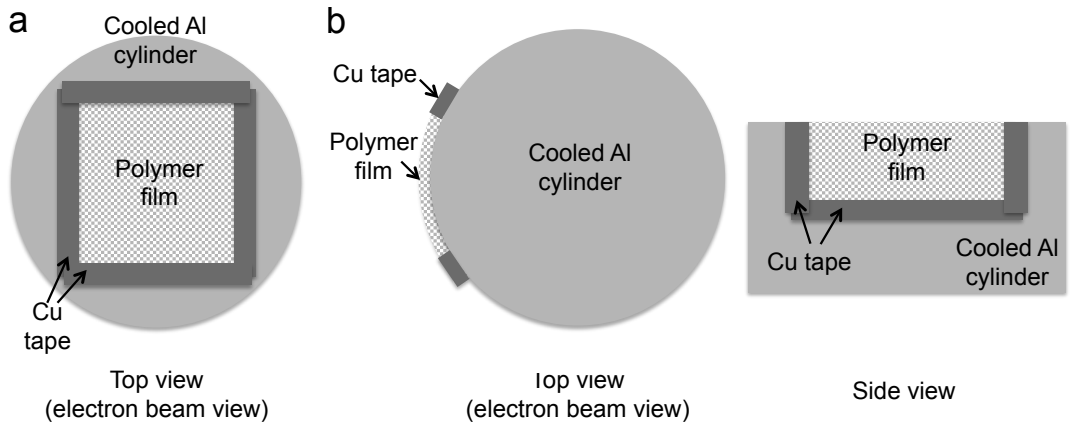

Figure 15. Schematic drawing of the setup used for *in situ* vapour sorption experiments in the ESEM, in surface mode (a) and in cross-section mode (b).

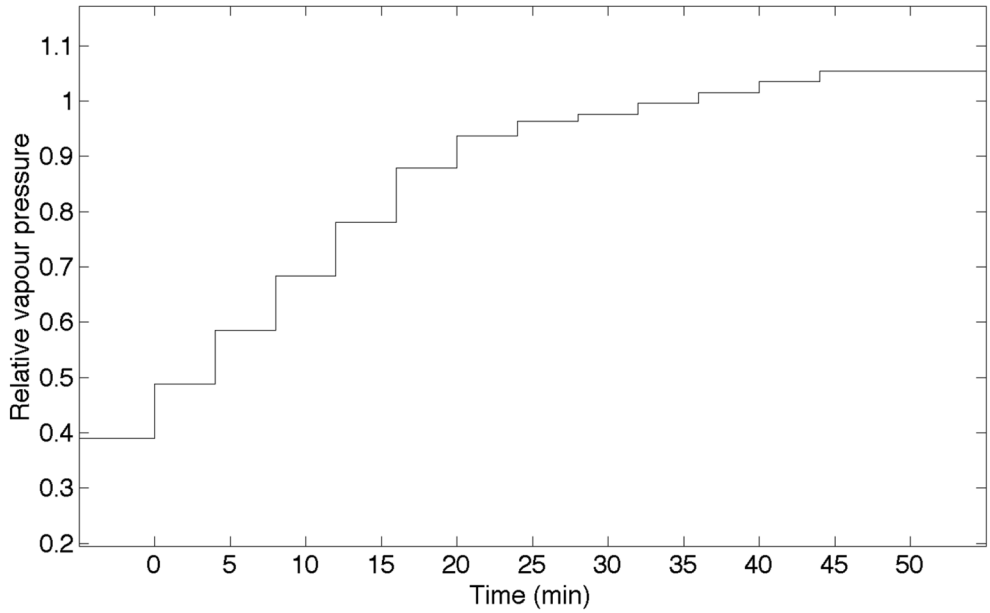

Figure 16. The protocol used for *in situ* vapour sorption experiments. The water vapour pressure was increased in a stepwise manner up to 5.10 torr (99% RVP) and 5.40 torr (105% RVP) in cross-section and surface mode, respectively. A smaller step size was used close to the condensation point. The holding time at each fixed pressure was 4 min.

Two different modes of the setup are shown in Figure 15. The cross-section mode was primarily used to measure the thickness change of films as a function of RH below 100% RH. In surface mode, the appearance of the film surface was studied as a function of RH. Here, the film was tightly sealed against the cylinder, precluding the possibility of water condensing underneath it. The pressure was increased above the condensation point to detect any droplet formation on the film surface (the term relative vapour pressure, RVP, was used here instead of RH as we cannot talk about relative humidity above 100%). The pressure required for condensation on the Al cylinder was 5.12 torr, i.e. slightly lower than the condensation pressure on the Cu cylinder in the wetting experiments on polymer films in paper IV (5.17 torr). This was accounted for in the calculation of the RH.

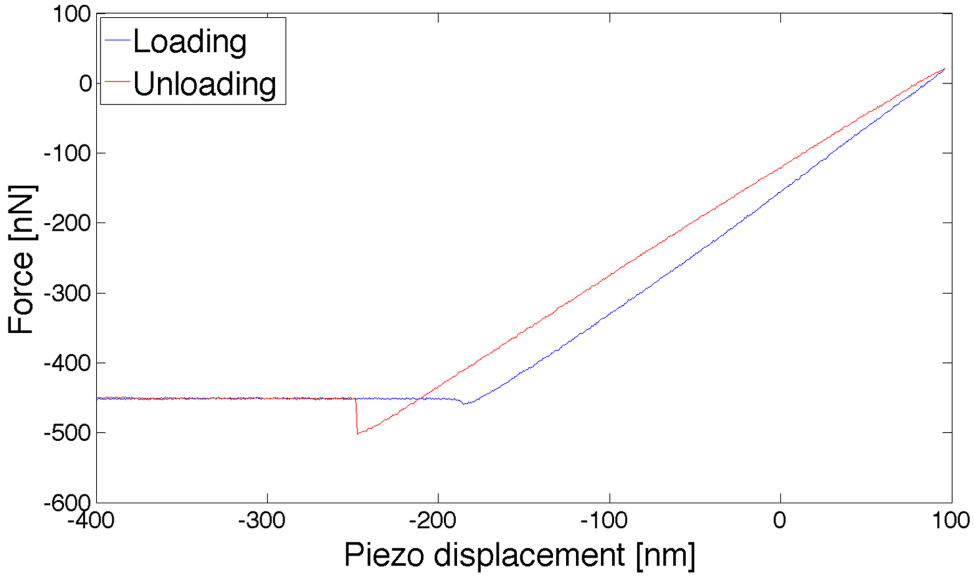

Figure 17. Example of a force-displacement curve obtained on a yeast cell at 66% RH in the ESEM.

4.4.2 In situ *force measurement for stiffness*

The calculation of Young's modulus of yeast cells at 66% RH is based on curves of force vs. piezo displacement where the sample is indented to an extent depending on its stiffness. An example of a force-displacement curve for a *P. pastoris* yeast cell is shown in Figure 17. It is linear and features a snap-out effect, visible in the unloading part of the curve.

Young's modulus for a single yeast cell was calculated by transforming the piezo displacement to sample indentation using the cantilever deflection on a hard undeformed surface (Weisenhorn *et al.*, 1993). The resulting force-indentation curve was then fitted to the Sneddon model for a cylindrical indenter (the choice of model is motivated in paper II). This model describes the force F acting on the cell as

$$F = 2R\frac{E}{1-\nu^2}\Delta z$$

where E is the Young's modulus of the cell, R the radius of the probe tip, ν the Poisson's ratio of the cell and Δz the indentation depth (Weisenhorn *et al.*, 1993). The Young's modulus was extracted from the coefficient.

5 MATERIALS AND SAMPLE PREPARATION

5.1 Cellulose fibres

The cellulose fibres used in the investigations originated from softwood kraft pulp provided by Södra Cell AB (Värö, Sweden). Two types of samples were used, differing in the way the fibres had been prepared. One of the batches had been mercerised, i.e. treated with sodium hydroxide (NaOH), reducing the hemicellulose content to approximately 9% of the dry weight of the pulp. The other batch contained a higher fraction of hemicellulose. Both batches were "never-dried" when obtained from the supplier, and they were stored in a refrigerator (below 8°C) to prevent drying and hornification prior to sample preparation.

Despite the fact that all fibres in a batch of pulp undergo the same treatment during the pulping process, there is typically a large variation in structure and properties among the fibres. This is important to point out as it has a bearing on the experimental results when it comes to water absorption and transport. There are several different properties that can vary from fibre to fibre. One important factor is what part of the tree stem the fibre originates from. The position in the radial direction of the stem determines the growth period during which the fibre was formed. This, in turn, is strongly related to its structure and function. As mentioned in section 2.1, *earlywood* is optimised for water transport while *latewood* is optimised for mechanical strength. At the fibre level, this means that earlywood fibres have a thinner cell wall and a larger lumen than latewood. The fibre morphology also varies as a function of genetic factors. There can be considerable variations between different individuals of a tree species as well as different parts of a stem – even within a single growth ring (Sjöström, 1993).

The pulps used for our investigations contained material from several different trees and from different parts of the stem. In light of the information above, one could therefore expect to see some variation in the appearance of different fibres and in their response to water exposure. No systematic study was made concerning the differences in properties between different fibres within a batch or between fibres from the different batches, as this was beyond the scope of the work in this thesis.

5.1.1 Preparation for in situ *microscopy*

To prepare a specimen for *in situ* microscopy, a single fibre was extracted from pulp using a pair of tweezers and glued to an Al wire with a diameter of 0.3 mm using epoxy resin. The longitudinal axis of the fibre was oriented along the axis of the wire. Scissors were used to cut the tip of the fibre; this was done to expose the lumen and make it accessible for water transport. The resin was allowed to cure at room temperature in air, during which time the fibre was exposed to dehydrating conditions. Hence, it should be pointed out that at the time of insertion into the microscope, the specimen was no longer moist.

5.2 Phase-separated polymer films

Ethyl cellulose (Ethocel™ Standard Premium) of viscosity grade 10 cP was supplied by Dow Wolff Cellulosics GmbH, Germany. Hydroxypropyl cellulose (Klucel® Pharm HPC) grade LF was supplied by Ashland, USA.

Free films of EC and HPC were produced by spraying a solution of 94% w/w ethanol (95%) and 6% w/w polymer onto a rotating drum according to a procedure described in the literature (Marucci *et al.*, 2009). The films were then peeled off the drum and stored in a desiccator. A film of pure EC as well as films with EC/HPC ratios of (w/w) 82/18, 78/22, 70/30 and 50/50 were prepared. These are referred to as EC100, HPC18, HPC22, etc., reflecting the film composition. In addition, a film of pure HPC, referred to as HPC100, was prepared using a modified spray-drying method (Marucci et al., 2013 (manufacturing)) and stored under the same conditions. The thickness of each film was measured in three different positions on the film. The mean thickness of EC100, HPC18, HPC22, HPC30, HPC50 and HPC100 was 0.09, 0.11, 0.11, 0.14, 0.12 and 0.12 mm, respectively.

5.2.1 HPC removal by pre-leaching

Samples of EC/HPC films where the HPC had been leached out were also used in the investigations. These samples will be referred to as "pre-leached". The leaching of films was done by immersion of the film in 700 ml of deionised water for 24 hours. The water was changed twice during this time and stirred at 80 rpm. Some film samples were embedded in epoxy and sectioned using an ultramicrotome (section 5.2.2) before leaching of the HPC in 500 ml of deionised water stirred at 250 rpm (the water was changed twice also here). The purpose of pre-leaching was (1) to enhance the visibility of the phase-separated morphology on the film surface or in the interior by removing the HPC, creating pores where the HPC used to reside or (2) to investigate by *in situ* wetting the water transport through the porous EC skeleton remaining after HPC leaching.

5.2.2 Exposing the internal microstructure

The microstructure in the interior of pure HPC and EC/HPC films was investigated in the ESEM and in the TEM. Exposing the internal microstructure required additional sample preparation and two different methods were used.

The first method was simply to scratch the surface of a pre-leached film sample with a pair of tweezers. This was done for HPC30 and HPC50 and it was possible because the integrity of the pre-leached samples was weakened due to the loss of HPC; for HPC50, simply handling the sample with tweezers damaged the surface layer. The specimens were imaged in low-vacuum mode in the ESEM and the view of the internal microstructure was parallel to the film surface.

In the second method, a (non-leached) film sample (HPC30, HPC50 and HPC100) was embedded in epoxy (Epoxy Rapid 332, Dana Lim, Denmark) and allowed to cure for at least 48 hours. The embedded sample was then sectioned using a Leica Ultracut UCT ultramicrotome (Leica, Germany) equipped with a diamond knife. After the first layers of material had been removed, a low sectioning speed was used in order to minimise smearing of the microstructure by the knife. The sections from HPC30 and HPC50 (nominally 500 nm and 100 nm thick, respectively) were placed between two Cu grids (3 mm diameter) for mechanical stability and investigated in the TEM in HAADF-STEM mode (paper IV). For the embedded film samples of HPC30, HPC50 and HPC100 remaining after sectioning, the exposed cross-sectional surfaces were imaged in low-vacuum mode in the ESEM.

Compared to the pre-leached samples, the porosity of the microtomed cross-sectional surfaces after HPC leaching was reduced, possibly due to smearing of the microstructure by the knife. However, the microtomed samples provide a useful comparison of the porosity before and after leaching and between different samples without the influence of a rough surface topography.

5.2.3 HPC rods

In addition to the polymer films, rod-shaped samples of HPC100 were used in the *in situ* ESEM experiments. These samples were intended as crude models of an idealised extended domain of HPC inside an EC/HPC film. The idealised HPC domain is imagined as a straight, HPC-filled channel of uniform thickness connecting the two sides of the EC/HPC film. For practical reasons, the rods had a much greater thickness than actual HPC domains in an EC/HPC film. Pieces of the HPC100 film were cut with scissors to a length of several millimetres. They had a rectangular cross section where one side had the thickness of the film (about 120 μm) and the other side had a thickness that varied between 20 μm and 100 μm for different samples. The rod-shaped specimens will henceforth be referred to as "HPC rods". Their purpose was to increase the understanding of the water movement into an HPC channel and the changes occurring in the HPC itself.

5.2.4 Preparation for in situ *microscopy*

Similar to the cellulose fibres, samples were prepared for *in situ* wetting experiments by attaching them to an Al wire with a diameter of 0.3 mm using epoxy resin. For film samples, rectangular pieces were attached in different orientations corresponding to the surface mode and the cross-section mode. For HPC rods, a sample was attached with its longitudinal axis along the axis of the wire, like the cellulose fibres. For *in situ* vapour sorption experiments, a rectangular film sample was attached to the Al cylinder using Cu tape. In the surface mode, all four edges of the sample were sealed against the cylinder by the tape. In the cross-section mode, three edges were taped while the fourth edge, facing the microscope pole piece, was left without tape in order to enable imaging of the film cross section.

5.3 Yeast cells

The yeast cells used in the measurements were *Pichia pastoris* wild type, obtained from Dr. Kristina Hedfalk at the University of Gothenburg (Gothenburg, Sweden) in the form of a suspension. The suspension had been prepared from a liquid cell culture where the yeast cells were grown in YPD (Yeast extract Peptone Dextrose). The rationale for choosing a liquid cell culture over an agar plate culture was based on the importance of a uniform cell population with respect to age and growth conditions for the sake of reproducibility of the experimental results.

5.3.1 Preparation for in situ *microscopy*

For the *in situ* ESEM experiments, the cell concentration of the suspension should be such that an appropriate amount of cells attach to the substrate. If the concentration is too high, cells will attach in clumps; if too low, very few cells will attach. To solve this problem, the optical density (OD) of the suspension was used as a guide. Since

previous examinations in a M.Sc. project (Ram, 2012) had shown that a suspension of optical density OD_{600}=2 resulted in an appropriate density of cells attached to the sample holder, the liquid cell culture was resuspended to OD_{600}=2. To ensure fresh samples, the experiments were performed within 24 hours of the preparation of the cell suspension. The Al wire used as a sample holder was immersed in the sample suspension for 30-60 s.

6 *IN SITU* WETTING OF INDIVIDUAL CELLULOSE FIBRES

The *in situ* sample stage was used for the wetting of individual cellulose fibres in paper I. The objectives were to evaluate the performance of the method and illustrate its possibilities, as well as study the interaction of an individual cellulose fibre with water.

An ESEM image of an individual cellulose fibre is shown in Figure 18(a). The fibre was cut with scissors to expose the lumen, which is visible in the image. For this particular specimen, the lumen appears to be open rather than collapsed. When several different fibres were examined with respect to their overall shape and structure, there was a considerable variation in the degree of collapse of the lumen and the tortuosity of the fibre. This probably reflects the mixed origin of the fibres in the batch where the samples were taken (section 5.1).

Figure 18 (b-d) shows an example of an *in situ* wetting experiment where a cellulose fibre makes contact with a water droplet on the vertical wall of the Cu cylinder, and the point of contact between the fibre and the droplet is visible. Swelling of the fibre

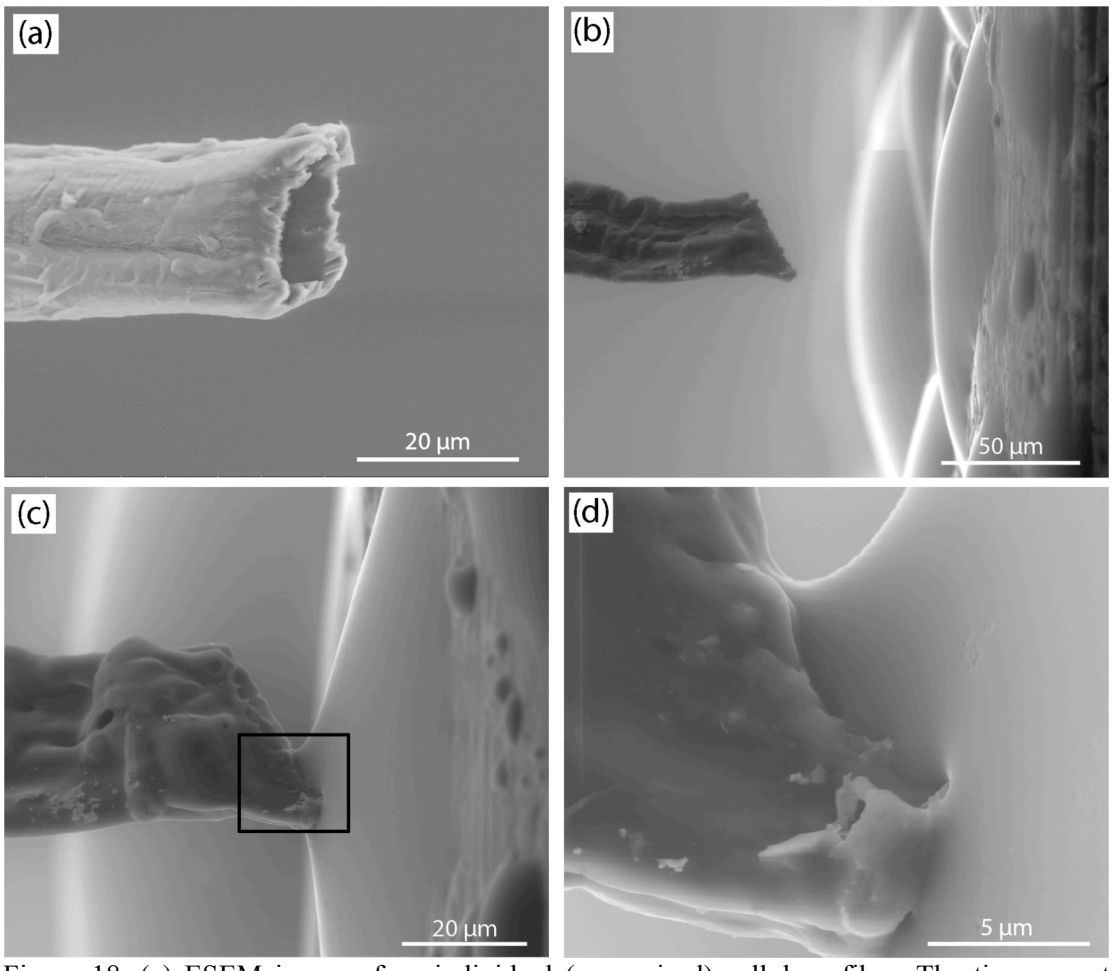

Figure 18. (a) ESEM image of an individual (mercerised) cellulose fibre. The tip was cut using scissors to expose the lumen. (b)-(d) ESEM images of a cellulose fibre approaching and making contact with a water droplet on the vertical wall of the Cu cylinder. The point of contact, highlighted by a box in (c), is shown at a higher magnification in (d).

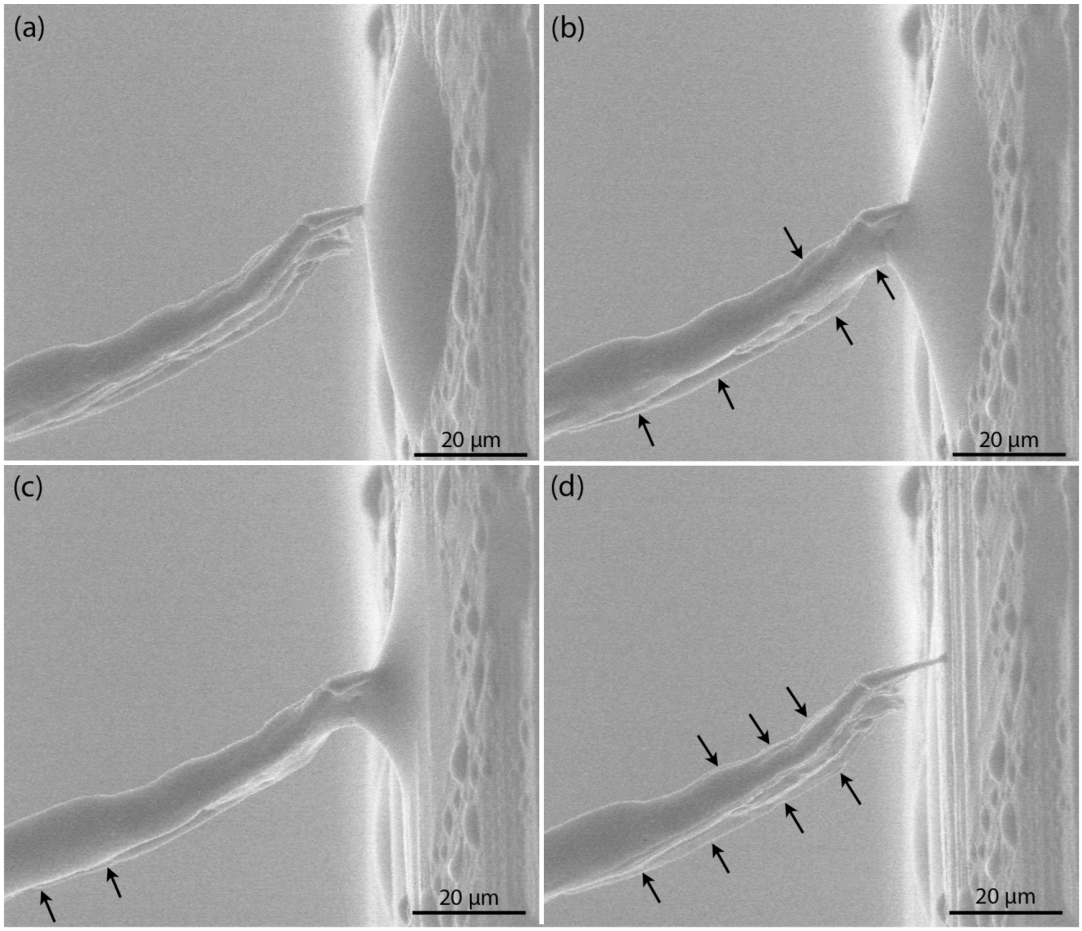

Figure 19. ESEM images from a movie showing how an individual cellulose fibre absorbs and transports a water droplet away from the surface of the Cu cylinder. During the process, the fibre shape changes as highlighted by arrows. It swells and then reverts back to its original shape.

was generally observed as an increase in thickness and a smoothening of surface topography. Swelling was observed to take place to some extent during approach toward the cylinder, prior to contact with the liquid water.

The series of images displayed in Figure 19 shows how an entire water droplet shrinks and disappears as it is put in contact with an individual cellulose fibre for an extended period of time. The images are selected frames from a movie that shows how the fibre swells before reverting back to its original shape. Arrows in the images of Figure 19 highlight this change in shape. The results indicate that the water droplet was absorbed and transported away from the surface of the Cu cylinder by the fibre. Several supporting arguments for this interpretation are presented in paper I. Moreover, the duration of the absorption process was about 15 s and the droplet volume was estimated to approximately 0.02 nL. An induction period of about 20 s took place before the major absorption event (after the image in (a) and before the image in (b)), and slight swelling of the fibre along with marginal shrinking of the droplet was observed during this period.

The experiment was repeated with several individual fibres, exhibiting a variation in absorptive capacity with respect to the time of absorption for different sized droplets as well as the number of droplets that could be absorbed in series before saturation

was reached. Again, the mixed origin of the fibres in the batch from which the samples were taken is believed to be the reason for this variation, as it may affect factors relevant to the absorptive capacity such as e.g. length, width, tortuosity and size/accessibility of lumen.

The temperature data presented in section 4.1.3 and the SVP curve in section 3.1 may be used to reason around the respective roles of the cell wall and the lumen in the wetting experiments. At 1 mm, which was approximately the maximum distance between the tip of the cellulose fibre and the Cu cylinder at the start of the experiment, the temperature is about 14°C. The initial water vapour pressure of 3.75 torr then gives an estimated RH of 30%. During approach toward the cylinder, the temperature decreases to about 6°C, increasing the RH to 70% just before contact with the liquid water. According to tables of the equilibrium moisture content (EMC) of wood (Glass & Zelinka, 2010), the moisture content increases from approximately 6% to 13% (of the ovendry mass) as the relative humidity increases from 30% to 70% at the temperatures used. These are equilibrium values; however, the time for moisture content equilibration decreases with decreasing size of the wood piece (Rowell, 2012). For a single cellulose fibre, we assume that the equilibration time is insignificant on the time scale of the experiment. As mentioned in section 2.1, the FSP is generally around 30% moisture content, although the value does vary somewhat (Glass & Zelinka, 2010). Thus, the induction period observed in the wetting experiment in Figure 19 may have been a consequence of the moisture content of the cell wall increasing toward the FSP before the lumen became engaged in water transport. After this induction period, the disappearance of the water droplet was mainly the result of capillary transport through the lumen of the fibre.

When working with water and materials in the ESEM, one has to consider the hydration state of the specimen at the start of the experiment. This may be affected by the sample handling and preparation prior to the investigation as well as by the pump-down procedure used to reach operating pressures in the sample chamber of the microscope. As mentioned in section 5.1, the preparation of the individual cellulose fibres involved a drying step to cure the epoxy resin. During this step, the fibres were exposed to dehydrating conditions for a prolonged period of time and, hence, subject to hornification as described in section 2.1. This most likely affected the fibre wall structure and, consequently, its capacity for absorption and swelling. Since the water content of the sample was relatively low at the time of insertion into the microscope, the pump-down step (which was carried out according to a gradual no-purge protocol as stated before) probably had only a minor influence, if any. It is doubtful if any alternative procedure could have maintained the moisture content of the fibre as it was in the never-dried pulp. The rate of drying of a single fibre, some 20-40 μm in diameter, should be high due to the large surface-to-volume ratio. The process of extracting an individual fibre from the pulp and mounting it on a sample holder takes at least several minutes, during which time the fibre most likely suffers some degree of hornification. A way of circumventing the problem could be to perform a solvent exchange of the never-dried pulp, after which the pulp can be dried in a special manner to avoid hornification (Köhnke *et al.*, 2010).

With the current sample preparation, the fibres retained sufficient swellability to enable the study of water transport in individual cellulose fibres using the developed technique. For the first time, direct and visual information on the water absorption by

a single, isolated cellulose fibre in real time is available. Studying a single fibre in isolation is valuable for the understanding of the fundamental interaction with water. In the future, the *in situ* wetting method may be used to study, for example, the water interaction of fibres with different processing history, the effects of hornification upon cyclic drying and rewetting *in situ* or the variation in transport properties in different directions of the fibre. As a next step, a sheet of fibres can be studied. The methodology for film geometry developed in the work on polymer films should be useful in this context.

7 *IN SITU* WETTING OF PHASE-SEPARATED POLYMER FILMS

Polymer films consisting of a phase-separated blend of EC and HPC were studied through *in situ* wetting in different orientations in the ESEM. The objectives were to (1) investigate the effect of the phase-separated microstructure on the water transport properties (paper III), and (2) gain insight into the dynamics and mechanisms of water transport during the initial stage of wetting of the films (paper IV), which has important implications on the hydration of coated oral formulations. *In situ* vapour sorption experiments in different orientations were used to obtain complementary information facilitating the interpretation of the wetting experiments. In addition to EC/HPC films, films of pure EC and pure HPC as well as HPC rods were studied in order to understand the water interaction of the materials constituting the EC/HPC films. The porosity of selected films was also examined in the ESEM and in the TEM in order to understand the effect of porosity on the water transport. Both studies (papers III and IV) contribute to a larger picture of the water interaction of EC/HPC films. This section provides a summary of the main results from the papers and some additional results from the work with EC/HPC films.

The microstructure of phase-separated EC/HPC films can be controlled by varying the polymer blend ratio, as explained in section 2.2. The structure at the film surface can be considerably different from that in the interior of the film. In Figure 20, the phase-separated morphology on the surface changes from discrete HPC domains in a continuous EC matrix for HPC18 and HPC22 to an almost bicontinuous appearance for HPC30 to discrete EC domains in a continuous HPC matrix for HPC50. Figure 21 reveals the internal microstructure of pre-leached HPC30 and HPC50. Pre-leached structures give a clear picture of the phase-separated morphology in the film interior since the pore volume was previously occupied by HPC. For HPC50, the structure appears truly bicontinuous and the pores (former HPC domains) are large compared to the length scale of the phase separation at the surface. Signs of the phase inversion observed at the surface are also visible in the interior, in the form of discrete spherical EC inclusions.

In paper III, the water transport properties of EC/HPC films with varying blend ratio were studied through *in situ* wetting experiments. The HPC fraction ranged from 18% to 50% w/w thus representing compositions below, around and above the threshold concentration for HPC percolation, which has previously been found to lie between 22% and 24% w/w (Marucci *et al.*, 2009). For the first time, direct visual information about the local water transport through phase-separated polymer films was obtained. Water penetrated all EC/HPC films in about 5 s and local variations in the time to penetration as well as the rate of penetration were observed. This information has a big impact on the understanding of the relationships between microstructure and transport properties, as spatially resolved information about the water transport on the length scale of the phase separation has not been available before. Also, the initial stage of wetting, where the polymer film goes from comparatively dry to wet, and the accompanying microstructure evolution has never been studied in detail before due to insufficient temporal resolution of traditional methods such as diffusion cell measurements.

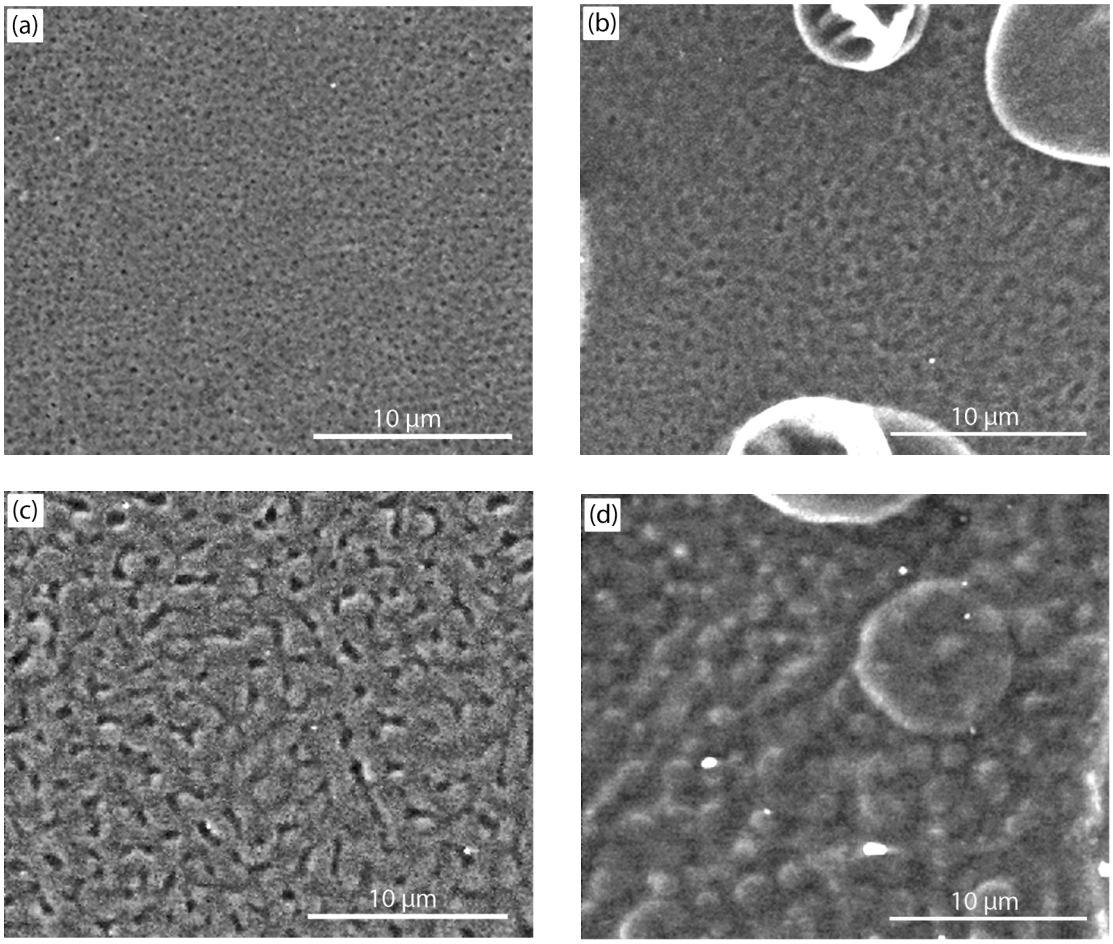

Figure 20. ESEM images of the microstructure at the surface of EC/HPC films with different polymer blend ratio: (a) HPC18, (b) HPC22, (c) HPC30 and (d) HPC50, recorded at the same magnification. In (b) and (d), residues from the spray-drying of the polymer solution during film formation are visible as round features larger than the EC and HPC domains.

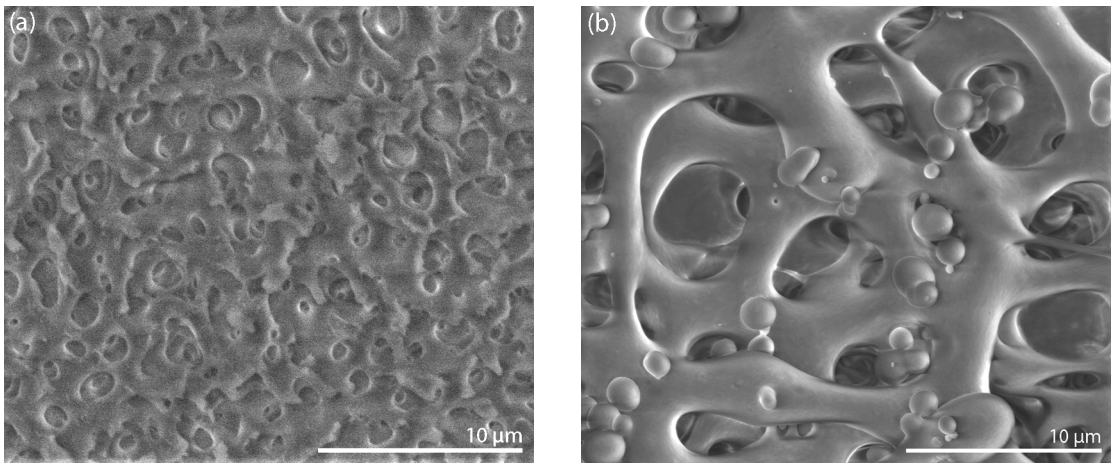

Figure 21. ESEM images of the internal microstructure of pre-leached HPC30 (a) and HPC50 (b), recorded at the same magnification. The structure was exposed through mechanical removal of the surface layer using tweezers and the viewing plane is parallel to the film surface. The pore volume was formerly occupied by HPC before leaching.

The results indicated that HPC18 had a few continuous HPC channels at places, connecting the two sides of the film, which may be expected thus close to the percolation threshold. The water transmission at 22% HPC was dramatically increased compared to 18%, reflecting the increased degree of percolation. A measure of the degree of percolation was also obtained by quantitative comparison of the inter-droplet distance with the inter-HPC-domain distance at the film surface. HPC30 had a higher degree of percolation than HPC22 as expected. For HPC50, entire regions of the surface, larger than the EC surface domains, were lifted up from underneath the surface due to swelling of HPC in the film.

7.1 Hydration dynamics and water transport mechanisms

In paper IV, *in situ* vapour sorption experiments showed that HPC swells to a much greater extent than EC in a humid environment. The restricted volume available for the swelling HPC in the film caused the formation of droplets (actually water-swollen HPC domains) on the surface of HPC30 at high RH. The absence of droplet formation on the surface of HPC50 under the same conditions was explained by the difference in microstructure at the surface as well as in the interior of the film and the consequent absence of the restricted-volume effect.

During the *in situ* wetting of HPC rods, the dissolution process occurred initially without the formation of a gel and left apparently undissolved material in the water reservoir. A region of solid swollen polymer ahead of the dissolution front indicated that the water penetration through HPC progressed faster than the dissolution front. The dissolution front progression over time was characterised by two distinct linear regimes and the transition between these regimes after 10-20 s was interpreted as a consequence of the swelling of the polymer in the solid state, which decreased the size of the water pathways and thus affected the speed of the dissolution front. A physical gel was formed after roughly 5-10 min, impeding further water intake due to a reduction of heterogeneities. Similarly, evidence of fast initial water penetration, relatively slow swelling and gel formation at longer time scales (within 15 minutes) were also observed during *in situ* wetting of EC/HPC films. Especially for HPC50, there was an obvious delay between the initial water penetration and the swelling of the HPC-continuous surface layer due to the absence of a restricted volume effect.

These observations were explained by a process described in the literature for polymers at low temperature (Ueberreiter, 1968) whereby water infiltrates pores on the molecular scale that exist in the polymer as a consequence of volume contraction during film formation when the polymer undergoes glass transformation. The penetrating water weakens the polymer structure at the points of lowest cohesion and enables dissolution through disintegration of the solid polymer. The swelling of the solid polymer after the initial water penetration as well as the formation of a gel that limits the water intake at longer time scales are also supported by this description. The dissolution profile is linear from the beginning of the wetting process due to the absence of gel formation. The phenomenon occurs specifically at low temperatures and short time scales before extensive polymer relaxation takes place, since time and water plasticisation (which lowers the glass transition temperature) are driving forces for polymer relaxation.

In support of this interpretation, TEM investigations of EC/HPC films provided evidence of pores up to a micrometre in size as well as indications of density variations. The density variations imply a spatially heterogeneous porosity on the nano scale or molecular scale. The pores and density variations were attributed to volume contractions and inhomogeneous polymer aggregation during film formation as the solvent evaporates. Density variations were also indicated in pure HPC by ESEM investigations.

Thus, the low temperature of the water in the ESEM seems to be responsible for the fast initial water transport through EC/HPC films *in situ*. The temperature dependence of the kinetics was checked by *ex situ* experiments and the result supported this explanation. The prevailing temperature gradient in the vicinity of the cold Cu cylinder may have had an effect in the case of the HPC rods, where water from the reservoir moved away from the cold surface as it invaded the rod, such that the increased temperature at a distance from the cylinder promoted polymer relaxation. However, gel formation was also observed at comparable time scales for the polymer films, which remained in contact with the water reservoir at the cold surface until they were retracted to observe the formed gel. Therefore, it was concluded that the possible effect of the temperature gradient did not constitute a conceptual difference between the polymer relaxation dynamics in the HPC rods and those in the HPC channels of the EC/HPC films.

These results led to a coherent picture of the mechanisms of water transport through EC/HPC films in the initial stage of wetting in the ESEM in paper IV. The initial water penetration occurs though pores on the nano scale and/or molecular scale in low-density regions of percolating HPC domains as well as through larger pores. This can explain the observations in paper III. For example, the water transport through EC/HPC films seemed to be associated with percolating HPC domains and, at the same time, significant local variations in the growth rate of droplets on film surfaces were observed (most strikingly for HPC30). The fast-growing droplets were probably associated with the larger pores. Furthermore, the time to water penetration was approximately constant across the wide range of compositions studied in paper III, a result that may seem surprising considering the large variation in the length scale of the phase-separated structure with composition. This, too, can be explained. Since the very most initial water transport occurs predominantly through pores at a significantly smaller length scale, the speed of water penetration is determined by the size of these pores rather than by the phase separation length scale. In addition, the increased understanding of water transport and delayed swelling in pure HPC enabled a correct interpretation of the special wetting behaviour displayed by HPC50, whose lack of a restricted-volume effect makes it behave more like pure HPC than do films with lower HPC content.

Interesting topics for further *in situ* ESEM studies on the EC/HPC system include the effect of the molecular weight of HPC on the dynamics of the water interaction of EC/HPC films as well as the wetting of oral formulations where a pellet has been coated with an EC/HPC film. In order to characterise the three-dimensional microstructure and the connectivity of the HPC domains as well as the intrinsic porosity, tomography in the TEM and serial block face SEM (SBF-SEM) (Reingruber *et al.*, 2011) could be used to probe the different length scales.

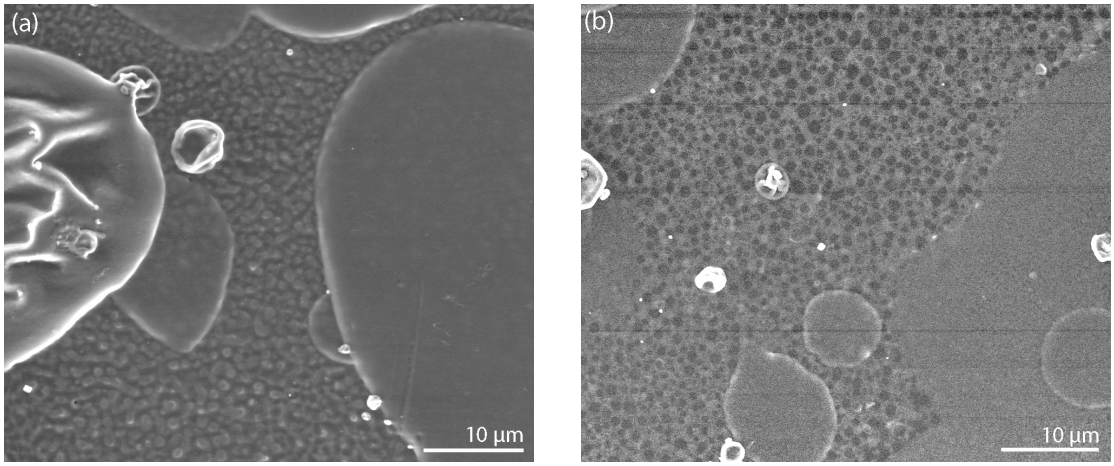

Figure 22. ESEM images of the surface of HPC50 from an *in situ* vapour sorption experiment, recorded at (a) 30% RVP and (b) 100% RVP (at different locations on the surface). In (a), HPC appears darker than EC. In (b), HPC appears lighter than EC due to preferential water sorption in HPC affecting the secondary electron emission. Residues from the spray-drying of the polymer solution during film formation are visible in some places.

7.2 Contrast mechanisms and electron beam interactions

An aspect of fundamental importance for the ESEM studies of EC/HPC films is the contrast between EC and HPC in secondary electron (SE) mode. SE imaging is sensitive to topographical variations but contrast may also arise between regions of different composition due to other mechanisms. Topographical as well as compositional contrast in polymer blend thin films has been demonstrated by AFM (Ramsdale *et al.*, 2002) and SE imaging in ESEM (Williams *et al.*, 2005). The topographical contribution was observed as a lighter rim along the phase boundary and was due to a height difference between the phases that gave rise to curvature at the boundary. The compositional contribution arose from a difference in stopping power (primary beam scattering) related to thickness variations. Topographical contrast was also observed by AFM on EC/HPMC films produced by spin coating, where HPMC domains were identified as pits (Lua *et al.*, 2007). In addition, charge contrast (Williams *et al.*, 2005) and SE-ion recombination contrast (Toth *et al.*, 2002) have been demonstrated in the ESEM.

The contrast between EC and HPC in our studies is a combination of topographical and compositional contrast, where the latter is the dominant contribution. The topographical contribution was mainly observed as a lighter rim along the phase boundary, probably due to a height difference between EC and HPC surface domains as described above. A height difference may be explained by differential shrinking of EC and HPC as the polymers undergo volume contraction upon solvent evaporation during film formation. The nature of the compositional contribution depended on the RH. At low RH, EC had a higher intensity than HPC, signifying a greater SE emission. At high RH, however, HPC attained a higher intensity than EC due to a higher water concentration. This resulted in a contrast reversal for HPC50, demonstrated in Figure 22. The contrast reversal was observed to occur at 50-60% RH. No dependence on scan rate was observed.

The origin of the compositional contrast is unclear but the most probable explanation is a difference in density between the phases. When examined using a gaseous backscattered electron detector, the phase-separated structure could not be observed,

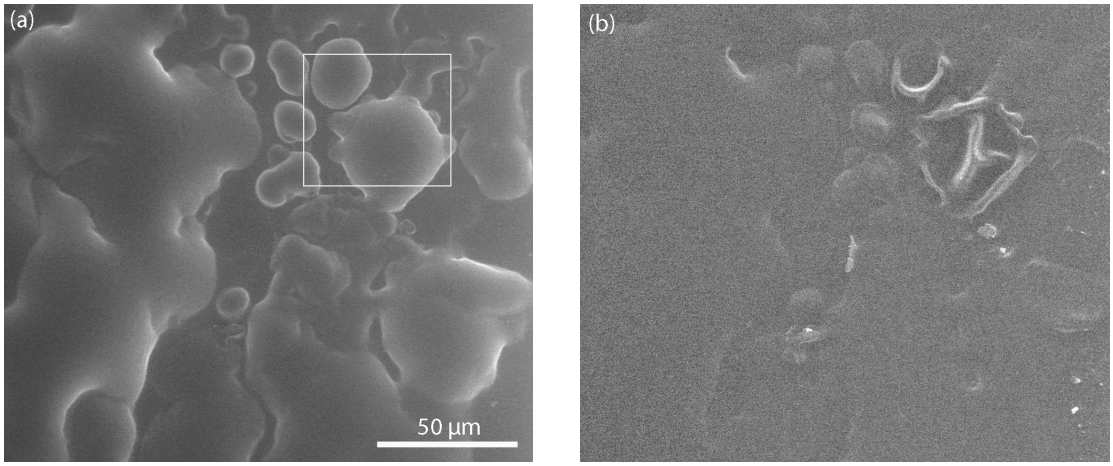

Figure 23. ESEM images of the surface of HPC30 during an *in situ* wetting experiment (a) before and (b) after *in situ* evaporation of water from the surface. The region highlighted by a box in (a) was previously exposed to the electron beam at higher magnification for several minutes. In (b), the HPC solution has a different appearance on this part of the surface than on the surrounding surface, indicating an effect of the previous beam exposure.

indicating that there was no significant difference in backscattered electron emission between the phases. The density of each phase, however, is influenced by e.g. molecular packing and degree of crystallinity. Such properties are likely to differ between EC and HPC, as they are related to molecular parameters such as the substitution type, the bulkiness of side groups attached to the cellulose backbone and specific interactions between groups on neighbouring molecules. The density affects the primary beam scattering and possibly also the SE mean free path in the material. At high RH, the water in HPC affects the interactions with the primary beam and/or the SE generated in the material such that the SE emission is increased and the contrast between EC and HPC reversed.

A specific type of electron beam interaction takes place in the aqueous solution of HPC that is formed on the surface of an EC/HPC film during *in situ* wetting in the ESEM. The consequence can be seen in Figure 23 for a part of the film surface that was exposed to the electron beam at relatively high magnification for an extended period of time during the initial stage of wetting. This is probably the result of chemical crosslinking of HPC molecules in the solution by the electron beam. Electron beam irradiation can induce irreversible changes in cellulose ethers, and the processes are affected by polymer concentration and irradiation dose. In solid state, the main reaction is chain cleavage caused by radiation-induced radicals on the macromolecules. In aqueous solution, the action of intermediate products of water radiolysis as well as the increased mobility of macromolecules can accelerate the radiation-induced chemical reactions. Radicals from water radiolysis react with the macromolecules and form macroradicals. When an HPC solution of moderate or high concentration is irradiated, an insoluble gel can be formed through the recombination of such macroradicals (Wach *et al.*, 2002).

In our experiments, it is likely that such an insoluble HPC gel is formed as a "shell" on the surface of solution droplets irradiated at a relatively high magnification. This can explain the less extensive droplet growth and coalescence observed in areas that have been irradiated for extended periods of time during the early stages of wetting

(paper III). *In situ* evaporation causes a decrease in the thickness of the droplets and a collapsed shell remains of the exposed droplets.

8 SWELLING AND STIFFNESS OF SINGLE YEAST CELLS

The *in situ* sample stage was used for experiments on single *P. pastoris* wild-type yeast cells in the ESEM. The objective was to verify a method for quantitative evaluation of the time-dependent expansion of an individual yeast cell due to osmotic shock. An increase in RH around the cell was used to create a situation analogous to a hyposmotic shock, where water migrates into the cell across the cell membrane due to the increased water potential on the outside. Cell size changes were measured locally on the cell surface using the AFM sensor and correlated with the changes in pressure. In addition, Young's moduli of yeast cells were extracted from force-displacement curves. Figure 24 shows an ESEM image of a yeast cell in contact with the AFM tip. A few other cells are also visible in the image.

Cell expansion was measured for two individual yeast cells as the water vapour pressure was increased from 3.5 to 4.8 torr, corresponding to an increase in RH from 66% to 90%. The result is displayed in Figure 25, where both the expansion and the pressure are plotted as a function of time. The pressure increase results in an expansion of both cells, which appear to stabilise at 120 and 150 nm expansion, respectively. The response is very fast in the initial stage and follows the pressure peak as the pressure overshoots its target value during the first 20 s. The responses of the two cells thus look qualitatively similar to each other.

The final expansion values were compared with the expansion observed in images of the cells from before and after the experiment (the cells were approximated as spheres). It was found that the expansion measured by the AFM sensor was somewhat higher than indicated by the images. The reason is that the depth of the indentation in the cell wall caused by the pressure from the AFM sensor depends on the Young's modulus which, in turn, depends on the turgor pressure in the cell. The turgor pressure increases as the cell absorbs water and swells (Arfsten *et al.*, 2010). The indentation depth is therefore reduced through the swelling process, contributing to the local expansion measured by the AFM sensor at the point of contact. This effect can be

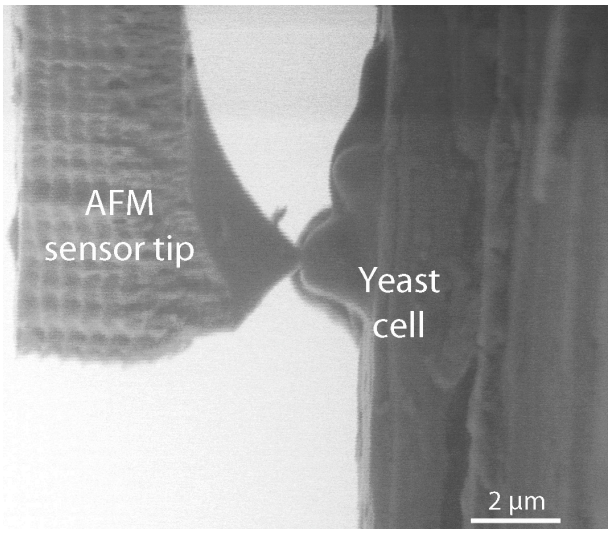

Figure 24. ESEM image of a yeast cell in contact with the AFM tip at 66% RH. The cell has a bud (daughter cell) that can be seen next to it in the image, and a few other cells are also visible behind these two.

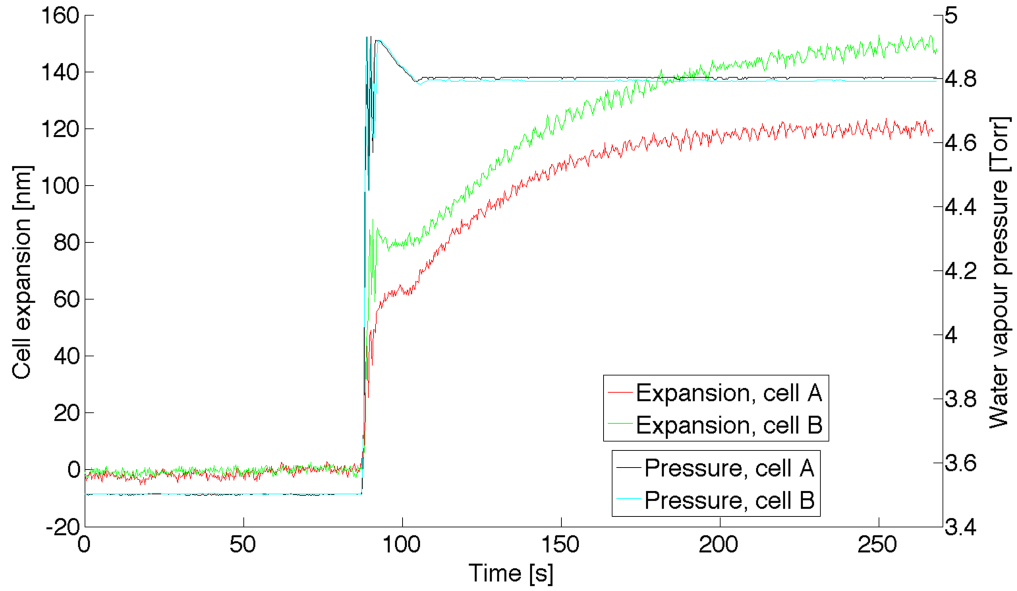

Figure 25. The expansion of two yeast cells A and B as a function of time, and the water vapour pressure as a function of time. The pressure is increased from 3.5 to 4.8 torr at about 87 s, corresponding to a change in RH from 66% to 90%.

avoided if a cantilever with a low spring constant is used, allowing the AFM tip to follow the cell expansion without indentation.

The response of yeast cells to osmotic chock is usually studied in aqueous media, where an osmotic shock can be induced by changing the osmolality of the medium. In the ESEM, we have an environment where the RH is used to simulate a hyposmotic shock. The export of solutes into the surrounding medium is part of the cell's strategy in coping with osmotic swelling, and this ability may be lost in a gaseous environment. However, our focus is on the immediate effects of cell swelling and how it is affected by the presence and activity of water channels in the cell membrane. The strong cell wall encloses the plasma membrane (Schaber *et al.*, 2010) and thereby the proteins embedded in it. It is therefore reasonable to assume that the aquaporins in the plasma membrane retain their structure and function in the gaseous environment of the ESEM. As a result, the *in situ* ESEM method is promising for the study of mechanosensitive (pressure-induced) regulation of aquaporin channels, a mechanism suggested in previous works (Soveral *et al.*, 2008; Fischer *et al.*, 2009). The ability to characterise individual cells with a high sensitivity to size changes also makes it highly interesting as a complementary tool for screening of drugs directed toward the water transport activity of cells.

The next steps toward successful implementation of the technique is to repeat the experiments with a cantilever of lower spring constant to avoid indentation effects, and to continue the investigation beyond the wild type strain by using engineered strains with different water transport properties. An important aspect is to establish a measurable and significant difference in the response between cells where the aquaporins have been deleted and wild type cells with native aquaporin expression or cells where the aquaporins have been overexpressed.

In addition to the measurement of cell swelling, the Young's moduli of the yeast cells were extracted from force-displacement curves. For cells A and B we obtained

Young's moduli of 13 and 15 MPa, respectively. These values are in the same range as earlier results on the yeast *Saccharomyces cerevisiae* (Lanero *et al.*, 2006; Ahmad *et al.,* 2008; 2010).

The piezoresistive AFM sensor provides the advantage of a direct and continuous force transduction that does not rely on imaging. It enables the measurement of cell size changes in the nanometre range and at the millisecond time scale. There are examples of other systems that combine AFM force probing with ESEM to study the mechanical and adhesion properties of yeast cells (Ahmad *et al.*, 2008; 2010; Shen, 2011) but these methods rely on image post-analysis to determine the force from the deflection of the AFM cantilever during indentation. Extracting force-deformation data by image analysis can be time-consuming (Stenson, 2010) and the image quality sometimes limits the possibility to extract the desired information (Ren *et al.*, 2008). The temporal resolution of imaging is limited by the maximum scanning speed that can be tolerated without compromising image quality. This is perhaps a minor limitation for the extraction of mechanical properties such as the Young's modulus by image post-analysis but a much greater one for the measurement of cell swelling at high spatial and temporal resolution. Moreover, the fact that our extraction of force-deformation data is independent of imaging also allows us to use a relatively low electron beam acceleration voltage, which is beneficial for cell viability.

The method for *in situ* force measurement can also be applied to other materials and research questions than the one described here, for example the swelling of other hydrated soft materials or, more generally, the measurement of mechanical forces on objects or structures down to the nanometre range such as the contact force between two nanoparticles.

9 CONCLUSIONS AND FUTURE OUTLOOK

In this work, new *in situ* ESEM methods for the study of the water interaction with soft materials have been developed and applied to three different materials systems: cellulose fibres, phase-separated polymer films and yeast cells. The aim was to enable and demonstrate new types of experiments that provide novel and useful information about the dynamic interaction of soft materials with water, especially with regard to water transport and structure dynamics in the material. An experimental platform, the *in situ* sample stage, was developed based on the combination of a nanomanipulator and a design for local cooling of a site readily accessible to the nanomanipulator.

The application of the developed methods to the different materials systems showed that the setup is flexible with respect to specimen shape and geometry and that the technique can be used to study several types of water interaction including water transport, swelling and dissolution. Especially for water transport, the standard wetting approach of the ESEM is limited and the presented *in situ* wetting method opens up new possibilities by offering control and visibility of the point of interaction between water and specimen. The simultaneous probing of microstructure and local water transport facilitates the correlation between structure and transport properties. For local and time-dependent swelling of materials structures, the sensitivity of measurements in the ESEM is enhanced by the use of a piezoresistive force sensor integrated with the *in situ* sample stage. This method eliminates the dependence on imaging resolution and scan speed, which can limit the spatial and temporal resolution of the swelling measurement, and uses the imaging capability of the ESEM mainly to locate and probe suitable measurement sites.

The *in situ* ESEM methods were used to (1) image the absorption and transport of liquid water in individual cellulose fibres, (2) investigate the relationships between microstructure and local water transport properties for phase-separated polymer (EC/HPC) films of varying composition, (3) elucidate the mechanisms of water transport through the polymer films in the ESEM and (4) measure size changes in the nanometre range in single yeast cells under simulated hyposmotic shock in the ESEM with a high temporal resolution. The results provide novel information about the materials and demonstrate the potential of the developed methods.

Further applications of the methods to the studied materials were suggested. Examples include studies of the effects of hornification on the wetting properties of individual cellulose fibres, the wetting properties of fibre networks, the effect of HPC molecular weight on the dynamics of water interaction in EC/HPC films, the wetting of coated pellets, mechanosensitive regulation of aquaporins in yeast cells and single-cell studies of the effectiveness of potential new drugs intended to affect the water transport activity of cells. The developed methods can also be applied to other materials systems where the interaction with water is of interest and, thus, can become an important technique in the ESEM *in situ* toolbox.

REFERENCES

Ahmad, M. R., Nakajima, M., Kojima, S., Homma, M. & Fukuda, T. (2008). In situ single cell mechanics characterization of yeast cells using nanoneedles inside environmental SEM. *IEEE Transactions on Nanotechnology, 7* (5), 607-616.

Ahmad, M. R., Nakajima, M., Kojima, S., Homma, M. & Fukuda, T. (2010). Nanoindentation methods to measure viscoelastic properties of single cells using sharp, flat, and buckling tips inside ESEM. *IEEE Transactions on Nanobioscience, 9* (1), 12-23.

Alink, R., Gerteisen, D. & Mérida, W. (2011). Investigating the Water Transport in Porous Media for PEMFCs by Liquid Water Visualization in ESEM. *Fuel Cells, 11* (4), 481-488.

Andersson, H. Hjärtstam, J., Stading, M., von Corswant, C. & Larsson, A. (2013). Effects of molecular weight on permeability and microstructure of mixed ethyl-hydroxypropyl-cellulose films. *European Journal of Pharmaceutical Sciences, 48,* 240-248.

Andreasson, B., Forsström, J. & Wågberg, L. (2003). The porous structure of pulp fibres with different yields and its influence on paper strength. *Cellulose, 10*, 111-123.

Arfsten, J., Leupold, S., Bradtmöller, C., Kampen, I., Kwade, A. (2010). Atomic force microscopy studies on the nanomechanical properties of Saccharomyces cerevisiae. *Colloids and Surfaces B: Biointerfaces, 79* (1), 284-290.

Blanco, N., Reidy, M., Arroyo, J. & Cabib, E. (2012). Crosslinks in the Cell Wall of Budding Yeast Control Morphogenesis at the Mother-Bud Neck. *Journal of Cell Science, 125* (23), 5781-5789.

Boissier, C., Feidt, F, & Nordstierna, L. (2012). Study of pharmaceutical coatings by means of NMR cryoporometry and SEM image analysis. *Journal of Pharmaceutical Sciences, 101* (7), 2512-2522.

Brown, G. & Chakrabarti, A. (1993). Phase separation dynamics in off-critical polymer blends. *Journal of Chemical Physics, 98,* 2451-2458.

Camacho-Bragado, G. A., Dixon, F. & Colonna, A. (2011). Characterization of the response to moisture of talc and perlite in the environmental scanning electron microscope. *Micron, 42* (3), 257-262.

Chinnan, M. S. & Park, H. J. (1995). Effect of plasticizer level and temperature on water vapor transmission of cellulose-based edible films. *Journal of Food Process Engineering, 18* (4), 417-429.

Côté, W. A. (1967). *Wood Ultrastructure.* Seattle: University of Washington Press.

Danilatos, G. D. & Brancik, J. V. (1986). Observation of liquid transport in the ESEM. In G. W. Bailey (Ed.), *Proceedings of the 44th Annual Meeting of the Microscopy Society of America.* San Francisco: San Francisco Press.

Donald, A. M., He, C., Royall, C. P., Sferrazza, M., Stelmashenko, N. A. & Thiel, B. L. (2000). Applications of environmental scanning electron microscopy to colloidal aggregation and film formation. *Colloids and Surfaces A: Physicochemical and Engineering Aspects, 174* (1-2), 37-53.

Dragnevski, K. I. & Donald, A. M. (2008). An environmental scanning electron microscopy examination of the film formation mechanism of novel acrylic latex. *Colloids and Surfaces A: Physicochemical and Engineering Aspects, 317* (1-3), 551-556.

Duchesne, I., Takabe. K. & Daniel, G. (2003). Ultrastructural localisation of glucomannan in kraft pulp fibres. *Holzforschung, 57* (1), 62-68.

Dufek, M. & Hayles, M. (2003). *The Quanta FEG 200, 400, 600 User's Operation Manual*. First edition. FEI Company.

Fernandes Diniz, J. M., Gil, M. H. & Castro, J. A. (2004). Hornification - Its origin and interpretation in wood pulps. *Wood Science and Technology, 37* (6), 489-494.

Ferrero, C., Massuelle, D. & Doelker, E. (2010). Towards elucidation of the drug release mechanism from compressed hydrophilic matrices made of cellulose ethers. II. Evaluation of a possible swelling-controlled drug release mechanism using dimensionless analysis. *Journal of Controlled Release, 141* (2), 223-233.

Fischer, G., Kosinska-Eriksson, U., Aponte-Santamaría, C., Palmgren, M., Geijer, C., Hedfalk, K., Hohmann, S., de Groot, B. L., Neutze, R. & Lindkvist-Petersson, K. (2009). Crystal structure of a yeast aquaporin at 1.15 angstrom reveals a novel gating mechanism. *Public Library of Science Biology, 7* (6).

Frohoff-Hülsmann, M. A., Lippold, B. C. & McGinity, J. W. (1999). Aqueous ethyl cellulose dispersion containing plasticizers of different water solubility and hydroxypropyl methyl-cellulose as coating material for diffusion pellets II: Properties of sprayed films. *European Journal of Pharmaceutics and Biopharmaceutics, 48* (1), 67-75.

Gennemark, P. (2005). Modeling and identification of biological systems with emphasis on osmoregulation in yeast. *Doktorsavhandlingar vid Chalmers tekniska högskola*. Gothenburg: Chalmers University of Technology.

Glass, S. V. & Zelinka, S. L. (2010). In *Wood handbook - Wood as an engineering material.* Madison: US Department of Agriculture, Forest Service, Forest Products Laboratory.

Goponenko, A. V., Boyle, B. J., Jahan, K. I., Gerashchenko, M. V., Fomenko, D. E., Gladyshev, V. N. & Dzenis, Y. A. (2011). Use of environmental scanning electron

microscopy for in situ observation of interaction of cells with micro- and nanoprobes. *Micro and Nano Letters, 6* (8), 603-608.

Grillitsch, K., Tarazona, P., Klug, L., Wriessnegger, T., Zellnig, G., Leitner, E., Feussner, I. & Daum. G. (2014). Isolation and characterization of the plasma membrane from the yeast Pichia pastoris. *Biochimica et Biophysica Acta, 1838* (7), 1889-1897.

Harris, M. & Ghebre-Sellassie, I. (2008). Aqueous polymeric coating for modified-release oral dosage forms. In J. W. McGinity & L. A. Felton (Eds.), *Aqueous polymeric coatings for pharmaceutical dosage forms*. CRC Press.

Hjärtstam, J. & Hjertberg, T. (1999). Studies of the water permeability and mechanical properties of a film made of an Ethyl Cellulose–Ethanol–Water ternary mixture. *Journal of Applied Polymer Science, 74* (8), 2056-2062.

Jenkins, L. M. & Donald, A. M. (1997). Use of the environmental scanning electron microscope for the observation of the swelling behaviour of cellulosic fibres. *Scanning, 19* (2), 92-97.

Jenkins, L. M. & Donald, A. M. (1999). Contact angle measurements on fibers in the environmental scanning electron microscope. *Langmuir, 15* (22), 7829-7835.

Jenkins, L. M. & Donald, A. M. (2000). Observing fibers swelling in water with an environmental scanning electron microscope. *Textile Research Journal, 70* (3), 269-276.

Karlsson, J. O., Andersson, M., Berntsson, P., Chihani, T. & Gatenholm, P. (1998). Swelling behavior of stimuli-responsive cellulose fibers. *Polymer, 39* (16), 3589-3595.

King, L. S., Kozono, D. & Agre, P. (2004). From structure to disease: The evolving tale of aquaporin biology. *Nature Reviews Molecular Cell Biology, 5* (9), 687-698.

Klipp, E. N. (2005). Integrative model of the response of yeast to osmotic shock. *Nature Biotechnology, 23* (8), 975-982.

Köhnke, T., Lund, K., Brelid, H. & Westman, G. (2010). Kraft pulp hornification: A closer look at the preventive effect gained by glucuronoxylan adsorption. *Carbohydrate Polymers, 81* (2), 226-233.

Laivins, G. & Scallan, V. (1993). The mechanism of hornification of wood pulps. In C. Baker (Ed.), *Products of papermaking*. Oxford: Pirs International.

Lanero, T., Cavalleri, O., Krol, S., Rolandi, R. & Gliozzi, A. (2006). Mechanical properties of single living cells encapsulated in polyelectrolyte matrixes. *Journal of Biotechnology, 124* (4), 723-731.

Larez-V, C., Crescenzi, V. & Ciferri, A. (1995). Phase Separation of Rigid Polymers in Poor Solvents. 1. (Hydroxypropyl)cellulose in Water. *Macromolecules, 28* (15), 5280-5284.

Lecomte, F., Siepmann, J., Walther, M., MacRae, R. J. & Bodmeier, R. (2003). Blends of enteric and GIT-insoluble polymers used for film coating: Physicochemical characterization and drug release patterns. *Journal of Controlled Release, 89* (3), 457-471.

Lindstedt, B., Sjöberg, M., Hjärtstam, J. (1991). Osmotic pumping release from KCl tablets coated with porous and non-porous ethylcellulose. *International Journal of Pharmaceutics, 67* (1), 21-27.

Lipke, P. N. & Ovalle, R. (1998). Cell Wall Architecture in Yeast: New Structure and New Challenges. *Journal of Bacteriology, 180* (15), 3735-3740.

Lua, Y., Cao, X., Rohrs, B. R. & Aldrich, D. S. (2007). Surface Characterizations of Spin-Coated Films of Ethylcellulose and Hydroxypropyl Methylcellulose Blends. *Langmuir*, 23 (8), 4286-4292.

Löwen, H., Watzlawek, M., Likos, C. M., Schmidt. M., Jusufi, A., Dzubiella, J., von Ferber, C., Allahyarov, E., Thünemann, A. & D'Amico, I. (2000). The Hard Physics of Soft Matter. *Advances in Solid State Physics, 40,* 809-817

Marechal, P., Martinez de Marafion, I., Molin, P. & Gervais, P. (1995). Yeast cell responses to water potential variations. *International Journal of Food Microbiology, 28* (2), 277-287.

Marucci, M., Hjärtstam. J., Ragnarsson, G., Iselau, F. & Axelsson, A. (2009). Coated formulations: New insights into the release mechanism and changes in the film properties with a novel release cell. *Journal of Controlled Release, 136* (3), 206-212.

Marucci, M., Arnehed, J., Jarke, A., Matic, H., Nicholas, M., Boissier, C. & von Corswant, C. (2013). Effect of the manufacturing conditions on the structure and permeability of polymer films intended for coating undergoing phase separation. *European Journal of Pharmaceutics and Biopharmaceutics, 83* (2), 301-306.

Montes-H, G., Geraud, Y., Duplay, J. & Reuschle, T. (2005). ESEM observations of compacted bentonite submitted to hydration/dehydration conditions. *Colloids and Surfaces A (Physicochemical and Engineering Aspects), 262* (1-3), 14-22.

Nafari, A. (2010). Microsensors for In Situ Electron Microscopy Applications. *Doktorsavhandlingar vid Chalmers tekniska högskola*. Gothenburg: Chalmers University of Technology.

Nafari, A., Karlen, D., Rusu, C., Svensson, K., Olin, H. & Enoksson, P. (2008). MEMS sensor for in situ TEM atomic force microscopy. *Journal of MicroElectroMechanical Systems, 17* (2), 328-333.

Pasantes-Morales, H. & Cruz-Rangel, S. (2010). Brain volume regulation: Osmolytes and aquaporin perspectives. *Neuroscience, 168* (4), 871-884.

Perkins, E. L. & Batchelor, W. J. (2012). Water interaction in paper cellulose fibres as investigated by NMR pulsed field gradient. *Carbohydrate Polymers, 87* (1), 361-367.

Ram, A. (2012). M.Sc. thesis: *A Novel Method for the In-Situ Mechanical Characterization of Single Living Yeast Cells in an ESEM*. Gothenburg: Chalmers University of Technology.

Ramsdale, C. M., Bache, I., MacKenzie, J. D., Thomas, D. S., Arias, A. C., Donald, A. M., Friend, R. H. & Greenham, N. C. (2002). ESEM imaging of polyfluorene blend cross-sections for organic devices. *Physica E: Low-dimensional Systems and Nanostructures, 14*, 268-271.

Reingruber, H., Zankel, A., Mayrhofer, C. & Poelt, P. (2011). Quantitative characterization of microfiltration membranes by 3D reconstruction. *Journal of Membrane Science, 372* (1-2), 66-74.

Reingruber, H., Zankel, A., Mayrhofer, C. & Poelt, P. (2012). A new in situ method for the characterization of membranes in a wet state in the environmental scanning electron microscope. *Journal of Membrane Science, 399-400*, 86-94.

Ren, Y., Donald, A. M. & Zhang, Z. (2008). Investigation of the morphology, viability and mechanical properties of yeast cells in environmental SEM. *Scanning, 30* (6), 435-442.

Riste, T. & Sherrington, D. (1989). *Phase Transitions in Soft Condensed Matter*. New York: Plenum Press.

Rizzieri, R., Baker, F. S. & Donald, A. M. (2003). A tensometer to study strain deformation and failure behavior of hydrated systems via in situ environmental scanning electron microscopy. *Review of Scientific Instruments, 74* (10), 4423-4428.

Rowell, R. (2012). *Handbook of Wood Chemistry and Wood Composites*. Second Edition. CRC Press.

Sakellariou, P. & Rowe, R. C. (1995). Interactions in cellulose derivative films for oral drug delivery. *Progress in Polymer Science, 20* (5), 889-942.

Sakellariou, P., Rowe, R. C. & White, E. F. T. (1986). Polymer/polymer interaction in blends of ethyl cellulose with both cellulose derivatives and polyethylene glycol 6000. *International Journal of Pharmaceutics, 34,* 93-103.

Sakellariou, P., Rowe, R. C. & White, E. F. T. (1988). A study of the leaching/retention of water-soluble polymers in blends with ethylcellulose using torsional braid analysis. *Journal of Controlled Release, 7* (2), 147-157.

Schaber, J., Adrover, M. Á., Eriksson, E., Pelet, S., Petelenz-Kurdziel, E., Klein, D., Posas, F., Goksör, M., Peter, M., Hohmann, S. & Klipp, E. (2010). Biophysical

properties of Saccharomyces cerevisiae and their relationship with HOG pathway activation. *European Biophysics Journal, 39* (11), 1547-1556.

Seo, M. & Kumacheva, E. (2002). Response of adsorbed layers of hydroxypropyl cellulose to variations in ambient humidity. *Colloid and Polymer Science, 280* (7), 607-615.

Shen, Y., Nakajima, M. R., Ahmad, M., Kojima, S., Homma, M. & Fukuda, T. (2011). Effect of ambient humidity on the strength of the adhesion force of single yeast cell inside environmental-SEM. *Ultramicroscopy, 111* (8), 1176-1183.

Siepmann, F., Siepmann, J., Walther, M., MacRae, R. J. & Bodmeier, R. Polymer blends for controlled release coatings. *Journal of Controlled Release, 125* (1), 1-15.

Siggia, E. D. (1979). Late stages of spinodal decomposition in binary mixtures. *Physical Review A, 20* (2), 595-605.

Sjöström, E. (1993). *Wood Chemistry - Fundamentals and Applications*. Second edition. San Diego: Academic Press.

Smith, A. E., Zhang, Z., Thomas, C. R., Moxham, K. E. & Middelberg, A. P. (2000). The mechanical properties of Saccharomyces cerevisiae. *Proceedings of the National Academy of Sciences of the United States of America, 97* (18), 9871-9874.

Smits, G. J., Kapteyn, J. C., van den Ende, H., Klis, F. M. (1999). Cell wall dynamics in yeast. *Current Opinion in Microbiology, 2,* 348-352.

Somero, G. & Yancey, P. (1997). In J. J. Hoffman (Ed.), *Handbook of Physiology*. Oxford: Oxford University Press.

Soveral, G., Madeira, A., Loureiro-Dias, M. C. & Moura, T. F. (2008). Membrane tension regulates water transport in yeast. *Biochimica et Biophysica Acta - Biomembranes, 1778* (11), 2573-2579.

Stenson, J. D., Ren, Y., Donald, A. M. & Zhang, Z. (2010). Compression testing by nanomanipulation in environmental scanning electron microscope. *Experimental Techniques, 34* (2), 60-62.

Stokes, D. J. (2008). *Principles and Practice of Variable Pressure/ Environmental Scanning Electron Microscopy (VP-ESEM).* West Sussex: John Wiley & Sons Ltd.

Sudo, S. (2011). Dielectric Properties of the Free Water in Hydroxypropyl Cellulose. *Journal of Physical Chemistry B, 115* (1), 2-6.

Svensson, K., Jompol, Y., Olin, H. & Olsson, E. (2003). Compact design of a transmission electron microscope-scanning tunneling microscope holder with three-dimensional coarse motion. *Review of Scientific Instruments, 74* (11), 4945-4947.

Tamás, M. J., Karlgren, S., Bill, R. M., Hedfalk, K., Allegri, L., Ferreira, M., Thevelein, J. M., Rydström, J., Mullins, J. G. L. & Hohmann, S. (2003). A short

regulatory domain restricts glycerol transport through yeast Fps1p. *Journal of Biological Chemistry, 278* (8), 6337-6345.

Theliander, H., Paulsson, M. & Brelid, H. (2002). *Introduktion till massa- och pappersframställning.* Gothenburg: Chalmers University of Technology.

Thiel, B. L. & Donald, A. M. (1992). In situ mechanical testing of fully hydrated carrots (daucus carotd) in the environmental SEM. *Annals of Botany, 82* (6), 727-733.

Toth, M., Thiel, B. L. & Donald, A. M. (2002). On the role of electron-ion recombination in low vacuum scanning electron microscopy. *Journal of Microscopy, 205* (1), 86-95.

Ueberreiter, K. (1968). The solution Process. In J. Crank & G. S. Park (Eds.), *Diffusion in Polymers*. London & New York: Academic Press.

Verbalis, J. G. (2010). Brain volume regulation in response to changes in osmolality. *Neuroscience, 168* (4), 862-870.

Wach, R. A., Mitomo, H., Yoshii, F. & Kume, T. (2002). Hydrogel of Radiation-Induced Cross-Linked Hydroxypropylcellulose. *Macromolecular Materials and Engineering, 287* (4), 285-295.

Wei, Q., Mather, R. R., Fotheringham, A. F. & Yang, R. D. (2002). Observation of wetting behavior of polypropylene microfibers by environmental scanning electron microscope. *Journal of Aerosol Science, 33* (11), 1589-1593.

Wei, Q. F., Mather, R. R., Fotheringham, A. F., Yang, R. & Buckman, J. (2003*a*). ESEM study of oil wetting behaviour of polypropylene fibres. *Oil and Gas Science and Technology, 58* (5), 593-597.

Wei, Q. F., Mather, R. R., Fotheringham, A. F. & Yang, R. (2003*b*). Dynamic wetting of fibers observed in an environmental scanning electron microscope. *Textile Research Journal, 73* (6), 557-561.

Weisenhorn, A. L., Khorsandi, M., Kasas, S., Gotzos, V. & Butt, H. J. (1993). Deformation and height anomaly of soft surfaces studied with an AFM. *Nanotechnology, 4* (2), 106-113.

Williams, S. J., Morrison, D. E., Thiel, B. L. & Donald, A. M. (2005). Imaging of semiconducting polymer blend systems using environmental scanning electron microscopy and environmental scanning transmission electron microscopy. *Scanning, 27* (4), 190-198.

Williams, D. B. & Carter, C. B. (2009). *Transmission Electron Microscopy: A Textbook for Materials Science. Part 3: Imaging.* New York: Springer Science+Business Media.

Yakimets, I., Wellner, N., Smith, A. C., Wilson, R. H., Farhat, I., Mitchell, J. (2007). Effect of water content on the fracture behaviour of hydroxypropyl cellulose films

studied by the essential work of fracture method. *Mechanics of Materials, 39* (5), 500-512.

Öberg, F. & Hedfalk, K. (2012). Recombinant production of the human aquaporins in the yeast Pichia pastoris. *Molecular Membrane Biology, Early Online*, 1-17.

Östlund, Å., Köhnke, T., Nordstierna, L. & Nydén, M. (2009). NMR cryoporometry to study the fiber wall structure and the effect of drying. *Cellulose, 17* (2), 321-328.

ACKNOWLEDGEMENTS

Many people contributed to this work in different ways. I would like to express my gratitude to all of them.

My supervisor Prof. Eva Olsson, for your steady guidance and inspiring enthusiasm. Thank you for devoting your time and for sharing your knowledge, pushing me forward on the road to becoming a scientist. Your encouragement has meant a lot to me.

My assistant supervisors Dr. Stefan Gustafsson and Prof. Anne-Marie Hermansson, for your invaluable contributions to the projects all the way from ideas through results, evaluation and writing. Stefan, thank you also for your help with the TEM work.

My co-workers Docent Anke Sanz-Velasco, Docent Krister Svensson and Dr. Alexandra Nafari, for your enormous engagement in both the "yeast project" and the "cellulose fibre project". You have been absolutely essential for the realisation of the *in situ* ESEM methods. I have really enjoyed working with you, both inside and outside of the lab!

Docent Kristina Hedfalk at the Department of Chemistry and Molecular Biology, University of Gothenburg, for your involvement in the yeast project. Thank you for your time and patience with my questions about yeast cells, for supplying us with samples and for believing in our work.

Södra Cell AB, for a fruitful collaboration in the cellulose fibre project and for supplying the fibre samples. A special thanks to Dr. Caroline Löfgren, for discussions and support throughout the project.

AstraZeneca R&D in Mölndal – especially Dr. Catherine Boissier, Dr. Mariagrazia Marucci and Mark Nicholas, for our long-standing and fruitful collaboration in the EC/HPC project. Thank you for providing the samples, for our many discussions and for your support throughout the evaluation and writing. Mark, thank you also for your help with TEM sample preparation.

The VINN Excellence Center SuMo Biomaterials, for the opportunity to work with such fascinating materials and research questions. Thanks to all my SuMo colleagues, for constructive discussions and for creating a stimulating research environment!

The Materials Science Area of Advance at Chalmers and SOFT Microscopy at Chalmers, for providing an inspiring research environment.

Vinnova for financial support of our work through SuMo Biomaterials.

The Carnegie Foundation and the Swedish Research Council for financial support of the yeast project.

Nanofactory Instruments AB for collaboration in the method development and for invaluable help with the experimental equipment.

Abhilash Ram for your contribution to the yeast project through your M.Sc. thesis work.

Several valued discussion partners. Dr. Debbie Stokes, Daniel Phifer and Jonas Appelfeldt at FEI Company, for sharing your expertise on environmental scanning electron microscopy. Prof. Anette Larsson, Dr. Tobias Gebäck and Prof. Jan Swenson at Chalmers, for discussions of the water transport mechanisms in EC/HPC films. Dr. Niklas Lorén at Chalmers and SIK and Dr. Erich Schuster at SIK for advice on image analysis.

My colleagues in the Eva Olsson Group and at the Division of Materials Microstructure, as well as former colleagues from the Division of Microscopy and Microanalysis. You make work enjoyable and you never hesitate to lend a helping hand! I especially want to thank Dr. Anders Kvist, for your help with the microscopes and Ola Löfgren, for your help with computer issues. Nothing would work without you! Special thanks also to my office mate Torben Pingel. You make life in the office more fun and you have been a tremendous help in many ways!

Rune Johansson, for being “en klippa” in the workshop! Thank you for all your help in crafting (and recrafting!) parts of the experimental equipment.

My beloved family: Mamma, Steffo, Jessica, Jimmy, Mormor and Berit. You have always supported and encouraged me, and for that I am deeply thankful! Heartfelt thanks for helping both Robert and me to manage our busy lives by taking fantastic care of our daughter! And Mormor, we also greatly appreciate your help around the house! ☺

Finally, my dearest Vilma and Robert. You are the world to me. Together, we finally made it through this challenge. I so look forward to spending more time with you from now on!